NASA TECHNICAL NOTE

NASA TN D-4274

FATIGUE OF LIQUID ROCKET ENGINE METALS AT CRYOGENIC TEMPERATURES TO -452° F (4° K)

by Alfred J. Nachtigall, Stanley J. Klima, and John C. Freche

Lewis Research Center
Cleveland, Ohio

NATIONAL AERONAUTICS AND SPACE ADMINISTRATION • WASHINGTON, D. C. • DECEMBER 1967

FATIGUE OF LIQUID ROCKET ENGINE METALS AT CRYOGENIC TEMPERATURES TO -452° F (4° K)

By Alfred J. Nachtigall, Stanley J. Klima, and John C. Freche

Lewis Research Center
Cleveland, Ohio

NATIONAL AERONAUTICS AND SPACE ADMINISTRATION

For sale by the Clearinghouse for Federal Scientific and Technical Information
Springfield, Virginia 22151 – CFSTI price $3.00

FATIGUE OF LIQUID ROCKET ENGINE METALS AT CRYOGENIC TEMPERATURES TO -452° F (4° K)

by Alfred J. Nachtigall, Stanley J. Klima, and John C. Freche

Lewis Research Center

SUMMARY

Axial tensile fatigue behavior of four candidate alloys for liquid rocket engines was investigated for smooth and notched (theoretical stress concentration factors $K_t > 17$) sheet specimens at a minimum-to-maximum cyclic stress ratio R of 0.14 in ambient air (70^o F, 294^o K), liquid nitrogen (-320^o F, 77^o K), and liquid helium (-452^o F, 4^o K). The materials tested were 2014-T6 aluminum alloy, Inconel 718, 5 percent aluminum - 2.5 percent tin - titanium (5Al-2.5Sn-Ti) alloy, and AISI 301 stainless steel.

The fatigue strength of smooth specimens was generally higher than that of notched specimens. Except for AISI 301 stainless steel, the fatigue strength of unnotched specimens increased progressively with decreasing test temperature to -452^o F (4^o K). This trend was also observed for 2014-T6 aluminum alloy and Inconel 718 in the notched condition. In most instances, Inconel 718 and 301 stainless steel had the highest fatigue strength while the 5Al-2.5Sn-titanium and 2014-T6 aluminum alloys ranked third and fourth. The titanium alloy generally had the highest fatigue-strength-to-density ratio at all temperatures.

The fatigue notch factor K_f increased with cyclic life for all materials at all test temperatures. Up to 100 cycles, the increase was small, and the fatigue notch factor was essentially equal to the tensile notch factor (ratio of smooth specimen tensile strength to notched specimen tensile strength). Inconel 718 generally had the lowest K_f over the life range considered at all temperatures.

The mode of fracture at all temperatures was generally transgranular for all materials. Minor phase particle cracking was associated with fatigue failure in 2014-T6 aluminum at all temperatures. The crack that caused fracture passed through and linked such particles. Although minor phase particle cracking was also observed in Inconel 718, the crack that caused fracture did not preferentially pass through the cracked particles. For the 5Al-2.5Sn-titanium alloy, deformation by slip and twinning was observed in both fatigue- and tensile-tested specimens. Twinning was particularly marked at -452^o F (4^o K).

INTRODUCTION

Cryogenic fluids play a major role in both aerospace and industrial applications. For example, liquid oxygen and liquid hydrogen are used as propellants in advanced rocket engines. To supply increased industrial needs, natural gas is converted to liquid form and transported from its source to the consumer, and liquid nitrogen is used as a refrigerant in the preservation of produce.

In all of these applications, because of the low temperatures involved, the mechanical properties of the container materials can be markedly affected. A better understanding of the behavior of materials at cryogenic temperatures is therefore needed to design properly for these various cryogenic applications.

Since rocket motor propellant tanks are subject to pressure fluctuations during the filling process as well as to vibratory stresses during use, their fatigue resistance is an important design criterion. Because of the difficulties associated with fatigue testing in cryogenic environments (specialized equipment, longtime tests, etc.), designers generally have had to use tensile test data as an indication of material behavior at cryogenic temperatures. A fairly comprehensive summary of cryogenic tensile test data for several classes of materials is given in references 1 to 13.

Some cryogenic fatigue data have also been obtained (refs. 13 to 23). Generally speaking, however, the extent of the fatigue data is limited, and much of it deals primarily with the high cyclic life region rather than the low cyclic life region. The low life region is of particular interest for rocket motor propellant tank design because pressure fluctuations may be accompanied by relatively high stresses and a correspondingly low cyclic life. Also, the vibratory stresses at launch, although of relatively short duration, may be high.

An investigation was conducted at the NASA Lewis Research Center to determine the cryogenic fatigue behavior of alloys representative of those used in tanks of liquid propellant rocket engines. Low cycle fatigue data were obtained under axial tension-tension loading ($R = 0.14$) with both smooth and notched sheet specimens of 2014-T6 aluminum alloy, Inconel 718, 5 percent aluminum - 2.5 percent tin - titanium alloy (5Al-2.5Sn-Ti), and AISI 301 stainless steel. Fatigue tests were conducted in ambient air at room temperature, in liquid nitrogen, and in liquid helium. Metallographic studies were made to relate fatigue behavior to metallurgical changes in the materials investigated.

MATERIALS, APPARATUS, AND PROCEDURE

Materials

The materials investigated were unclad 2014-T6 aluminum alloy, Inconel 718,

TABLE I. - CHEMICAL ANALYSES OF MATERIALS TESTED

Material	Base metal	Alloying elements, wt. %																		
		Copper	Chromium	Aluminum	Silicon	Iron	Tin	Nickel	Manganese	Columbium and tantalum	Carbon	Magnesium	Molybdenum	Nitrogen	Titanium	Oxygen	Zinc	Hydrogen	Phosphorous	Boron	Sulfur
2014-T6[a]	Aluminum	4.45	0.04	----	0.92	0.60	---	0.009	0.69	----	----	0.57	----	0.0012	0.02	[b]<0.0005	0.052	0.0004	-----	------	-----
Inconel 718[c]	Nickel	.05	18.1	0.57	.29	16.7	---	-----	.31	4.92	0.05	----	3.17	------	1.04	--------	-----	------	-----	0.0023	0.007
5Al-2.5Sn-Ti[c]	Titanium	----	-----	5.14	----	-----	2.6	-----	----	----	.016	----	----	.012	----	.59	-----	.0094	-----	------	-----
AISI 301 Stainless steel[a]	Iron	----	17.7	----	.34	-----	---	6.8	.84	----	.107	----	----	.049	----	.0022	-----	.001	0.016	------	-----

[a]Analysis supplied by independent laboratory.

[b]Not detectable.

[c]Analysis supplied by vendor.

TABLE II. - CONDITION OF MATERIALS PRIOR TO TESTING

Material	Condition
2014-T6 alloy	As received (unclad)
Inconel 718	Solution annealed at 1950° F (1339° K) for 1 hr; air cooled; aged at 1350° F (1006° K) for 9 hr; furnace cooled to 1200° F (922° K); held at 1200° F (922° K) for 9 hr; air cooled
5Al-2. 5Sn-Ti alloy	Mill annealed at 1325° F (922° K) for 4 hr; furnace cooled
AISI 301 Stainless steel	Cold rolled 60 percent

5Al-2. 5Sn-Ti alloy, and AISI 301 stainless steel. Chemical analyses of these alloys are given in table I. The conditions in which the materials were investigated are listed in table II.

Specimens

The specimens used for both tensile and fatigue tests were identical. The specimens were fabricated so that the direction of loading was parallel to the rolling direction for all materials except the aluminum alloy, for which the rolling direction was transverse to the axis of the specimen. Specimen geometry is shown in figure 1. The streamline fillet contour shown for the smooth specimen was chosen to minimize the occurrence of failures in the transition region between the specimen head and the test section. The streamline fillet contour was one of several suggested in reference 24. Smooth specimens were ground to this contour with a contour-shaped grinding wheel. The contoured edges of the test section were then polished with a hand polishing tool to remove all transverse grinding marks. Notches were first roughly ground. Then a sharpened broaching tool, ground to the desired angle of the V-notch, was drawn across the root of the notch to produce the required root radius. The latter operation was repeated until the specified test section dimension was achieved. The as-received sheet thickness of Inconel 718 was 0. 093 inch (2. 36 mm). Specimen thickness was reduced to 0. 080 inch (2. 03 mm) by hydrolapping the flat faces, which was done to ensure that a sufficiently wide range of stress levels could be obtained without exceeding the 10 000-pound (4536-kg)

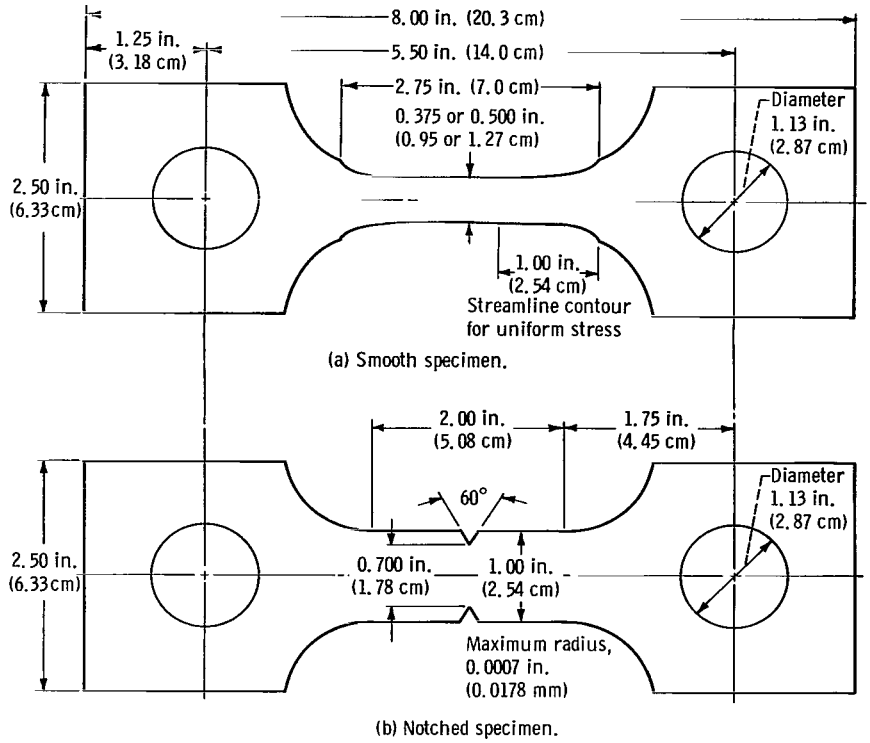

Figure 1. - Sheet tensile and fatigue specimens. Specimen thicknesses: 2014-T6 aluminum alloy, 0.060 inch (1.52 mm); Inconel 718, 0.080 inch (2.03 mm); 5 percent aluminum - 2.5 percent tin - titanium alloy, 0.020 inch (0.51 mm); 301 stainless steel, 0.022 inch (0.56 mm).

load capacity of the fatigue machine. The other sheet materials were tested in the as-received condition without surface preparation. Nominal specimen thicknesses were 0.060, 0.020, and 0.022 inch (1.52, 0.51, and 0.56 mm) for the aluminum alloy, titanium alloy, and stainless steel, respectively. These thicknesses were chosen for experimental convenience and availability. Generally they are representative of the sheet thicknesses employed in fluid containers of various rocket engines.

Apparatus

Tensile test apparatus. - The tensile tests were conducted in conventional universal testing machines. The cryostat used to contain the cryogenic fluid that surrounded the test specimen was essentially a double-walled, insulated cylindrical vessel, open at the top. The cryostat is described in reference 5.

Fatigue test apparatus. - A Krouse fatigue-testing machine, described in reference 25, was modified for use with a cryostat capable of operation with liquid helium. The major modifications to the machine consisted of (1) raising the upper crosshead on

taller columns to accommodate the cryostat height and (2) connecting the two loading arms of the machine with a crossbeam to combine the two 5000-pound (2268-kg) loading capacities of each side of the machine into a single 10 000-pound (4536-kg) loading capacity. In addition to the direct belt-driven speed of 1980 cycles per minute (33 Hz), separate motor-driven reduction gears were provided to permit operation at 200 and 16 cycles per minute (3.3 and 0.27 Hz, respectively).

The cryostat was specifically designed for this investigation and is shown in figure 2. It consisted of a vacuum-tight enclosure that surrounded a cylindrical specimen chamber.

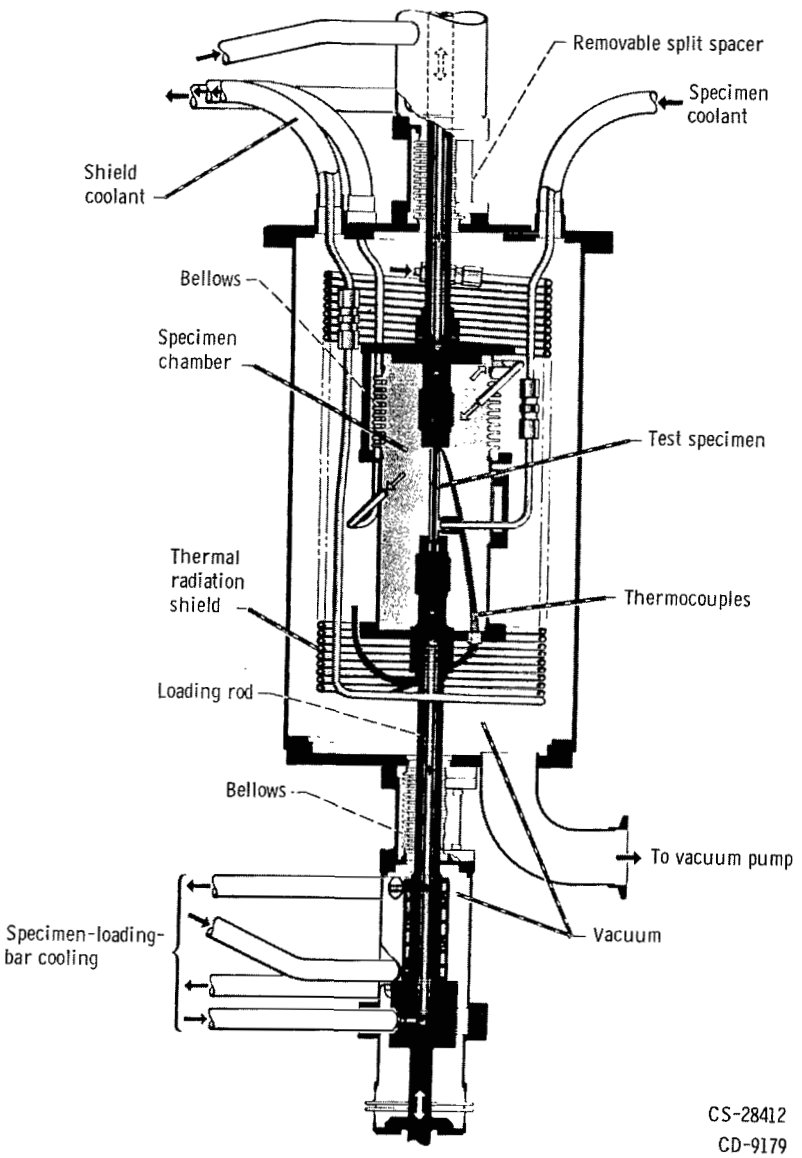

Figure 2. - Fatigue testing cryostat.

The chamber contained the cryogenic fluid in which the test specimen was immersed. A closely spaced coil containing liquid nitrogen served as a radiation shield during tests with liquid helium. The bellows permitted specimen and pull-rod motion to take place without loading the cryostat.

Instrumentation. - Copper-constantan thermocouples were clamped to the test specimens for the tests conducted in liquid helium. The reference junction was immersed in liquid nitrogen at atmospheric pressure. The thermocouple electromotive force was amplified and recorded on a strip chart recorder.

Procedure

Tensile tests. - Tensile tests were run at approximately 70° F (294° K) in ambient air, at -320° F (77° K) in liquid nitrogen, and at -423° F (20° K) in liquid hydrogen. The lowest tensile test temperature was limited to -423° F (20° K) because the cryostat lacked adequate insulation to retain liquid helium. At least three unnotched and three notched specimens of each material were tested at each temperature.

Fatigue tests. - Axial-tension fatigue tests were conducted with each material at an R factor of 0.14 at approximately 70° F (294° K), -320° F (77° K), and -452° F (4° K) (liquid helium). The maximum cyclic stress levels applied varied from near the tensile strength of the material to its endurance limit. The -320° F (77° K) and -452° F (4° K) tests were conducted by surrounding the specimens with liquid nitrogen and liquid helium, respectively. For long-life tests of the order of 10^4 cycles and higher, the cycling rate was 1980 cycles per minute (33 Hz). Shorter life tests were run either at 200 or 16 cycles per minute (3.3 or 0.27 Hz, respectively). For the range of cyclic frequencies used in this investigation, it was assumed that the effect of frequency on fatigue life was insignificant. A minimum of one and a maximum of six specimens were tested at each stress level considered. Stresses were always calculated on the basis of the minimum cross-sectional area of each specimen prior to testing.

Metallography. - Metallographic studies were made of specimens tested at each temperature for all materials. Macrographs and micrographs are presented. Microetching, X-ray diffraction, and electron-beam X-ray microanalysis techniques were employed to identify microstructural phases.

RESULTS AND DISCUSSION

Tensile and fatigue data for the four materials, 2014-T6 aluminum alloy, Inconel 718, 5Al-2.5Sn-Ti alloy, and 301 stainless steel are summarized in tables III and IV and are discussed in the first part of this section of the report. Metallurgical aspects related to these data are discussed in the latter part of this section.

TABLE III. - TENSILE PROPERTIES OF MATERIALS TESTED

Material	Temperature		Specimen configuration							
			Unnotched						Notched	
			Ultimate tensile strength, σ_u		Yield strength, 0.2 percent offset		Modulus of elasticity, E		Net tensile strength	
	°F	°K	lb/sq in.	N/sq cm	lb/sq in	N/sq cm	lb/sq in.	N/sq cm	lb/sq in.	N/sq cm
2014-T6 aluminum alloy	70	294	70.8×10^3	48.8×10^3	65.9×10^3	45.5×10^3	11.3×10^6	7.8×10^6	54.5×10^3	37.6×10^3
			71.4	49.2	66.1	45.6	10.6	7.3	57.4	39.6
			71.0	49.0	64.7	44.6	10.8	7.4	57.4	39.6
	Average		71.1×10^3	49×10^3	65.6×10^3	45.2×10^3	10.9×10^6	7.5×10^6	56.4×10^3	38.9×10^3
	-320	77	86×10^3	59.3×10^3	76.9×10^3	53.1×10^3	11.6×10^6	8.0×10^6	57.6×10^3	39.7×10^3
			86.1	59.4	77.7	53.6	11.1	7.7	56.9	39.2
			86.7	59.8	77.5	53.4	11.9	8.2	53.9	37.2
	Average		86.3×10^3	59.5×10^3	77.4×10^3	53.4×10^3	11.5×10^6	7.9×10^6	56.1×10^3	38.7×10^3
	-423	20	101.1×10^3	69.7×10^3	---	---	---	---	62.8×10^3	43.3×10^3
			100.8	69.5	84.1×10^3	58.0×10^3	12.0×10^6	8.3×10^6	59.9	41.3
			102.7	70.8	---	---	---	---	59.0	40.7
	Average		101.5×10^3	70.0×10^3	84.1×10^3	58.0×10^3	12.0×10^6	8.3×10^6	60.6×10^3	41.8×10^3
Inconel 718	70	294	179.5×10^3	123.8×10^3	150.0×10^3	103.4×10^3	30.3×10^6	20.9×10^6	180.5×10^3	124.5×10^3
			184.2	127.0	155.4	107.1	31.0×10^6	21.4×10^6	179.5	123.8
			189.4	130.6	---	---	---	---	188.5	130.0
	Average		184.4×10^3	127.1×10^3	152.7×10^3	105.3×10^3	30.7×10^6	21.2×10^6	182.8×10^3	126.0×10^3
	-320	77	243×10^3	167.5×10^3	185.3×10^3	127.8×10^3	32.8×10^6	22.6×10^6	208.8×10^3	144.0×10^3
			244.4	168.5	186.6	128.7	31.9	22.0	214.5	147.9
			237.0	163.4	175.7	121.1	32.6	22.5	215.2	148.4
			---	---	---	---	---	---	215.8	148.8
	Average		241.5×10^3	166.5×10^3	182.5×10^3	125.9×10^3	32.4×10^6	22.3×10^6	213.6×10^3	147.3×10^3
	-423	20	250.5×10^3	172.7×10^3	195.0×10^3	134.4×10^3	32.7×10^6	22.6×10^6	242.3×10^3	167.0×10^3
			265.4	183.0	---	---	---	---	225.0	155
			257.8	177.8	---	---	---	---	220.7	152.2
	Average		257.9×10^3	177.8×10^3	195.0×10^3	134.4×10^3	32.7×10^6	22.6×10^6	229.3×10^3	158.0×10^3

TABLE III. - Concluded. TENSILE PROPERTIES OF MATERIALS TESTED

Material	Temperature		Specimen configuration							
			Unnotched						Notched	
			Ultimate tensile strength, σ_u		Yield strength, 0.2 percent offset		Modulus of elasticity, E		Net tensile strength	
	°F	°K	lb/sq in.	N/sq cm	lb/sq in.	N/sq cm	lb/sq in.	N/sq cm	lb/sq in.	N/sq cm
5Al-2.5Sn-Ti alloy	70	294	108.2×10^3	74.6×10^3	102.7×10^3	70.8×10^3	16.6×10^6	11.5×10^6	126.6×10^3	87.3×10^3
			111.5	76.9	107.6	74.2	17.0	11.7	124.0	85.5
			107.5	74.2	102.5	70.7	16.0	11.0	128.8	88.8
			115.8	79.8	102.6	70.7	16.9	11.7	---	---
			113.0	77.9	107.7	74.3	16.2	11.2	---	---
	Average		111.2×10^3	76.7×10^3	104.6×10^3	72.1×10^3	16.5×10^6	11.4×10^6	126.5×10^3	87.2×10^3
	-320	77	183.4×10^3	126.4×10^3	177.8×10^3	122.6×10^3	17.7×10^6	12.2×10^6	177.8×10^3	122.6×10^3
			180.4	124.4	175.5	121.0	18.0	12.4	188.2	129.8
			179.4	123.7	172.0	118.6	17.6	12.1	177.0	122.0
			184.1	126.9	179.6	123.8	17.9	12.3	---	---
	Average		181.8×10^3	125.4×10^3	176.2×10^3	121.5×10^3	17.8×10^6	12.3×10^6	181.0×10^3	124.8×10^3
	-423	20	231.9×10^3	159.9×10^3	211.6×10^3	145.9×10^3	19.7×10^6	13.6×10^6	149.6×10^3	103.1×10^3
			220.5	152.0	---	---	---	---	132.0	91.0
			230	158.6	---	---	---	---	136.8	94.3
			228.4	157.5	207.4	143.0	18.0	12.4	---	---
			236.7	163.2	210.0	144.8	19.2	13.2	---	---
			228.8	157.8	210.7	145.3	16.7	11.5	---	---
	Average		229.4×10^3	158.2×10^3	209.9×10^3	144.8×10^3	18.4×10^6	12.7×10^6	139.5×10^3	96.1×10^3
AISI 301 Stainless steel	70	294	230.5×10^3	158.9×10^3	220.5×10^3	152.0×10^3	26.0×10^6	17.9×10^6	211.6×10^3	145.9×10^3
			238.0	164.1	221.0	152.4	25.0	17.4	227.0	156.5
			233.0	160.6	213.5	147.2	25.0	17.5	220.0	153.1
	Average		233.8×10^3	161.2×10^3	218.3×10^3	150.5×10^3	25.3×10^6	17.6×10^6	219.5×10^3	151.3×10^3
	-320	77	336.7×10^3	232.1×10^3	256.0×10^3	176.5×10^3	27.0×10^6	19.0×10^6	207.8×10^3	143.3×10^3
			335.3	231.2	262.0	180.6	26.0	18.3	207.8	143.3
			331.6	228.6	247.0	170.3	27.0	19.0	225.7	157.0
			---	---	---	---	---	---	216.2	149.1
			---	---	---	---	---	---	238.2	164.2
			---	---	---	---	---	---	217.6	150.0
	Average		334.5×10^3	230.6×10^3	255.0×10^3	175.8×10^3	26.7×10^6	18.8×10^6	218.9×10^3	151.2×10^3
	-423	20	340.1×10^3	234.4×10^3	287.4×10^3	197.8×10^3	28.0×10^6	19.0×10^6	193.5×10^3	133.4×10^3
			344.5	237.5	308.0	212.3	26.0	18.2	178.5	123.1
			329.2	227.0	---	---	---	---	180.5	124.5
			340.0	234.4	303.0	209.9	30.0	20.5	---	---
			333.0	229.6	---	---	---	---	---	---
	Average		337.3×10^3	232.6×10^3	299.5×10^3	206.7×10^3	28.0×10^6	19.2×10^6	184.2×10^3	127.0×10^3

TABLE IV. - SUMMARY OF FATIGUE RESULTS

(a) 2014-T6 aluminum alloy

Maximum cyclic stress, σ_{max}		Cycles to failure $\times 10^3$		Maximum cyclic stress, σ_{max}		Cycles to failure $\times 10^3$		Maximum cyclic stress, σ_{max}		Cycles to failure $\times 10^3$	
$lb/in.^2$	N/cm^2	Individual	Average	$lb/in.^2$	N/cm^2	Individual	Average	$lb/in.^2$	N/cm^2	Individual	Average
Test temperature, ^oF (^oK)											
70 (294)				-320 (77)				-452 (4)			
Unnotched specimens											
78.8×10^3	54.3×10^3	0.55	0.55	92.8×10^3	63.8×10^3	7.45 10.0	8.7	110.0×10^3	75.8×10^3	5.9	5.9
70.0×10^3	48.3×10^3	5.5 10.0 10.5	8.7	87.5×10^3	60.3×10^3	7.15 14.3 15.8	12.4	105.0×10^3	72.4×10^3	8.8 10.6	9.7
61.3×10^3	42.3×10^3	18.2 22.8 27.4	22.8	78.8×10^3	54.3×10^3	35.7 43.4	39.6	96.3×10^3	66.4×10^3	16.2 16.4	16.3
52.5×10^3	36.2×10^3	15.6 39.1 40.1 36.3 58.3	37.9	70.0×10^3	48.3×10^3	222.2	222.2	87.5×10^3	60.3×10^3	45.5 124.3	84.9
43.8×10^3	30.2×10^3	121.4 138.9 159.5	139.5	61.3×10^3	42.3×10^3	>1000.0	(a)	78.8×10^3	54.3×10^3	71.8	71.8
39.4×10^3	27.2×10^3	128.0 340.3	234.2					70.0×10^3	48.3×10^3	344.3 777.3	560.8
35.0×10^3	24.1×10^3	500.0 >3 200.0 >17 660.0	(a)								

Notched specimens											
52.5×10^3	36.2×10^3	0.002	(a)	52.5×10^3	36.2×10^3	0.044	0.044	52.5×10^3	36.2×10^3	0.062	(a)
		.013		43.8×10^3	30.2×10^3	0.19	0.37			.107	
		.040				.35		43.8×10^3	30.2×10^3	0.42	0.61
43.8×10^3	30.2×10^3	0.23	0.27			.56				.80	
		.24		35.0×10^3	24.1×10^3	2.22	2.33	35.0×10^3	24.1×10^3	1.26	2.66
		.28				2.43				4.05	
		.33		26.3×10^3	18.1×10^3	5.9	6.3	26.3×10^3	18.1×10^3	7.16	8.63
35.0×10^3	24.1×10^3	0.69	1.29			6.6				10.1	
		1.12		17.5×10^3	12.1×10^3	43.2	46.0				
		1.34				48.8					
		1.40									
		1.59									
		1.60									
26.3×10^3	18.1×10^3	3.40	4.75								
		4.00									
		4.00									
		5.30									
		5.70									
		6.10									
17.5×10^3	12.1×10^3	28.1	29.5								
		28.5									
		28.7									
		30.4									
		30.5									
		30.7									
8.8×10^3	6.1×10^3	148.0	150.6								
		153.2									
6.5×10^3	4.5×10^3	615.0	662.0								
		709.0									
4.4×10^3	3.0×10^3	>11 200.0	(a)								

[a]Individual points plotted in figures.

TABLE IV. - Continued. SUMMARY OF FATIGUE RESULTS

(b) Inconel 718

Maximum cyclic stress, σ_{max}		Cycles to failure $\times 10^3$		Maximum cyclic stress, σ_{max}		Cycles to failure $\times 10^3$		Maximum cyclic stress, σ_{max}		Cycles to failure $\times 10^3$	
lb/in.^{2}	N/cm^2	Individual	Average	lb/in.^{2}	N/cm^2	Individual	Average	lb/in.^{2}	N/cm^2	Individual	Average
Test temperature, ^{o}F (^{o}K)											
70 (294)				-320 (77)				-452 (4)			
Unnotched specimens											
196 $\times 10^3$	135.1$\times 10^3$	0.10	0.10	235 $\times 10^3$	162.0$\times 10^3$	4.1	4.1	245 $\times 10^3$	168.9$\times 10^3$	15.7	16.9
175	120.7	10.16	12.7	232.5$\times 10^3$	160.3$\times 10^3$	7.6	7.6		144.8$\times 10^3$	18.1	
		15.30									
140 $\times 10^3$	96.5$\times 10^3$	43.1	47.1	224 $\times 10^3$	154.4$\times 10^3$	34.7	34.7	210 $\times 10^3$		59.3	66.1
		51.0		210 $\times 10^3$	144.8$\times 10^3$	53.0	40.1			72.8	
105 $\times 10^3$	72.4$\times 10^3$	268.0	268.0			54.4		175 $\times 10^3$	120.7$\times 10^3$	208.7	214.4
91 $\times 10^3$	62.7$\times 10^3$	372.0	372.0			28.9				216.1	
84 $\times 10^3$	57.9$\times 10^3$	695.8	695.0			24.0		161 $\times 10^3$	111.0$\times 10^3$	408.0	408.0
				196 $\times 10^3$	135.1$\times 10^3$	63.0	90.9	154 $\times 10^3$	106.2$\times 10^3$	383.4	383.4
						118.8		140 $\times 10^3$	96.5$\times 10^3$	>1000.0	(a)
				175 $\times 10^3$	120.7$\times 10^3$	57.6	119.9				
						112.0					
						190.0					
				168 $\times 10^3$	115.8$\times 10^3$	124.4	154.4				
						184.4					
Notched specimens											
175 $\times 10^3$	120.7$\times 10^3$	0.26	0.26	175 $\times 10^3$	120.7$\times 10^3$	0.89	0.89	175 $\times 10^3$	120.7$\times 10^3$	1.02	1.02
140 $\times 10^3$	96.5$\times 10^3$	1.30	1.30	140 $\times 10^3$	96.5$\times 10^3$	2.58	2.58	140 $\times 10^3$	96.5$\times 10^3$	2.43	2.83
105 $\times 10^3$	72.4$\times 10^3$	4.20	4.20	105 $\times 10^3$	72.4$\times 10^3$	9.66	9.66			3.23	
63 $\times 10^3$	43.4$\times 10^3$	22.40	22.40	63 $\times 10^3$	43.4$\times 10^3$	37.4	37.4	105 $\times 10^3$	72.4$\times 10^3$	12.45	12.45
42 $\times 10^3$	29.0$\times 10^3$	165.70	165.70	42 $\times 10^3$	29.0$\times 10^3$	224.0	224.0	63 $\times 10^3$	43.4$\times 10^3$	55.9	55.9
28 $\times 10^3$	19.3$\times 10^3$	>1 126.0	(a)					42 $\times 10^3$	29.0$\times 10^3$	643.0	643.0
								28 $\times 10^3$	19.3$\times 10^3$	>1000.0	(a)

(c) 5Al-2.5Sn-titanium alloy

Unnotched specimens											
122.5×10^3	84.5×10^3	0.3	(a)	180×10^3	124.1×10^3	9.1	9.1	220×10^3	151.7×10^3	1.7	1.7
		4.9		157.5×10^3	108.6×10^3	30.8	30.8	210×10^3	144.8×10^3	15.8	22.3
		7.9		140×10^3	96.5×10^3	47.8	47.8			28.7	
113.8×10^3	78.5×10^3	16.4	30.4	122.5×10^3	84.5×10^3	100.0	100.0	192.5×10^3	132.7×10^3	14.8	22.2
		29.7		113.8×10^3	78.5×10^3	103.2	122.1			22.5	
		36.5				140.9				29.2	
		38.9						175×10^3	120.7×10^3	43.2	53.3
105×10^3	72.4×10^3	40.4	64.6	105×10^3	72.4×10^3	>10 000.0	(a)			40.6	
		40.7								76.1	
		87.7						140×10^3	96.5×10^3	169.4	179.5
		89.4								189.6	
96.3×10^3	66.4×10^3	137.6	199.1					126×10^3	86.9×10^3	277.6	280.5
		260.5								283.4	
87.5×10^3	60.3×10^3	209.5	(a)								
		>11 237.7									
78.8×10^3	54.3×10^3	>10 516.5	(a)								
70.0×10^3	48.3×10^3	>10 422.3	(a)								
Notched specimens											
122.5×10^3	84.5×10^3	0.25	0.24	179.9×10^3	124.0×10^3	0.012	(a)	140×10^3	96.5×10^3	0.014	0.014
		.22				.042		122.5×10^3	84.5×10^3	0.176	0.203
105×10^3	72.4×10^3	0.62	0.67	175×10^3	120.7×10^3	0.130	0.130			.230	
		.72		157.5×10^3	108.6×10^3	0.230	0.230	105×10^3	72.4×10^3	0.310	0.566
87.5×10^3	60.3×10^3	1.5	1.6	126.2×10^3	87.0×10^3	0.820	0.820			.400	
		1.7		105×10^3	72.4×10^3	1.59	1.59			.632	
70×10^3	48.3×10^3	3.3	3.6	87.5×10^3	60.3×10^3	3.03	3.03			.920	
		3.9		$70.\times10^3$	48.3×10^3	5.9	5.9				
52.5×10^3	36.2×10^3	7.4	7.6	52.5×10^3	36.2×10^3	11.2	11.2				
		7.7									
35×10^3	24.1×10^3	20.4	22.7								
		25.0									
17.5×10^3	12.1×10^3	597.4	(a)								
		>5 688.0									

[a]Individual points plotted in figures.

TABLE IV. - Concluded. SUMMARY OF FATIGUE RESULTS

(d) AISI 301 Stainless steel

Maximum cyclic stress, σ_{max}		Cycles to failure $\times 10^3$		Maximum cyclic stress, σ_{max}		Cycles to failure $\times 10^3$		Maximum cyclic stress, σ_{max}		Cycles to failure $\times 10^3$	
$lb/in.^2$	N/cm^2	Individual	Average	$lb/in.^2$	N/cm^2	Individual	Average	$lb/in.^2$	N/cm^2	Individual	Average
Test temperature, ^oF (^oK)											
70 (294)				-320 (77)				-452 (4)			
Unnotched specimens											
245 $\times 10^3$	168.9×10^3	5.3	5.3	336 $\times 10^3$	231.7×10^3	2.0	2.0	343 $\times 10^3$	236.3×10^3	0.015 1.57	(a)
239.8×10^3	165.3×10^3	5.2	5.2	323.8×10^3	223.3×10^3	2.6	2.6	336 $\times 10^3$	231.7×10^3	1.33	1.33
236.3×10^3	162.9×10^3	5.9	5.9	315 $\times 10^3$	217.2×10^3	3.5	3.5	330 $\times 10^3$	206.7×10^3	1.10 1.33	1.22
231 $\times 10^3$	159.3×10^3	11.2	11.2	280 $\times 10^3$	193.1×10^3	6.2 11.0	8.6	315 $\times 10^3$	217.2×10^3	1.32 1.40	1.36
210 $\times 10^3$	144.8×10^3	10.4 11.2	10.8	245 $\times 10^3$	168.9×10^3	16.8	16.8	280 $\times 10^3$	193.1×10^3	4.20 4.83	4.52
175 $\times 10^3$	120.7×10^3	47.3 66.3	56.8	210 $\times 10^3$	144.8×10^3	49.5	49.5	245 $\times 10^3$	168.9×10^3	7.00 7.34 10.57	8.30
140 $\times 10^3$	96.5×10^3	83.7 124.9 185.9	131.5	175 $\times 10^3$	120.7×10^3	120.3	120.3	210 $\times 10^3$	144.8×10^3	7.80 8.31 10.49 14.80 20.38	12.36
122.5×10^3	84.5×10^3	449.5 >5 649.4 >8 468.5	(a)	140 $\times 10^3$	96.5×10^3	240.5	240.5	175 $\times 10^3$	120.7×10^3	15.70 18.20 37.50	23.8
105 $\times 10^3$	72.4×10^3	103.4 >16 163.7	(a)	122.5×10^3	84.5×10^3	>1000	(a)	157.5×10^3	108.6×10^3	45.9 86.7	66.3
								140 $\times 10^3$	96.5×10^3	>1000.0	(a)

Notched specimen											
210×10^3	144.8×10^3	0.018	0.018	210×10^3	144.8×10^3	0.035 .040	0.038	192.5×10^3	132.7×10^3	0.022	0.022
192.5×10^3	132.7×10^3	0.080 .088	0.084	192.5×10^3	132.7×10^3	0.052 .055 .083	0.063	157.5×10^3	108.6×10^3	0.090 .098	0.094
157.5×10^3	108.6×10^3	0.322 .346	0.334	157.5×10^3	108.6×10^3	0.420 .480	0.450	122.5×10^3	84.5×10^3	0.376 .406	0.391
122.5×10^3	84.5×10^3	1.48 1.75 2.26	1.83	122.5×10^3	84.5×10^3	2.32 1.99	2.16	87.5×10^3	60.3×10^3	1.30 1.74	1.52
87.5×10^3	60.3×10^3	5.8 6.7 6.9 7.3 7.4 8.0	7.0	87.5×10^3	60.3×10^3	7.8	7.8				
52.5×10^3	36.2×10^3	27.9 29.5 29.6 30.2 30.5 31.5	29.9	52.5×10^3	36.2×10^3	27.4 33.0	30.2				
35×10^3	24.1×10^3	58.7 73.2	66.0								
17.5×10^3	12.1×10^3	>8 220.1	(a)								

[a]Individual points plotted in figures.

Tensile Data

Figure 3 presents a bar chart comparison of smooth and notched tensile data at 70° F (294° K) in ambient air, at -320° F (77° K) in liquid nitrogen, and at -423° F (20° K) in liquid hydrogen for all four materials investigated. Generally, the stainless steel was the strongest material and the aluminum alloy the weakest at all test temperatures. Three of the materials, 2014-T6, Inconel 718, and 301 stainless steel were notch sensitive at all test temperatures; that is, the tensile strength of notched specimens was lower than the tensile strength of smooth specimens. The degree of notch sensitivity for all materials usually increased as the temperature decreased. The 5Al-2. 5Sn-Ti alloy was notch sensitive only at -423° F (20° K). At 70° F (294° K) the notch tensile strength of this alloy was higher than the unnotched tensile strength, and at -320° F (77° K) the tensile strengths of smooth and notched specimens were equal. Apparently a transition from ductile to brittle behavior occurs for this alloy between -320° F (77° K) and -423° F (20° K). These results are similar to those shown in reference 11 for another heat of this alloy, also with low interstitial content.

Figure 3 also shows that the tensile strength of smooth specimens progressively increased as temperature decreased. The only exception was stainless steel at -423° F (20° K). A similar trend of continuously increasing strength with decreasing temperature for notched specimens occurred only for Inconel 718. It is interesting to note that, although the stainless steel had the highest strengths at all temperatures in the unnotched

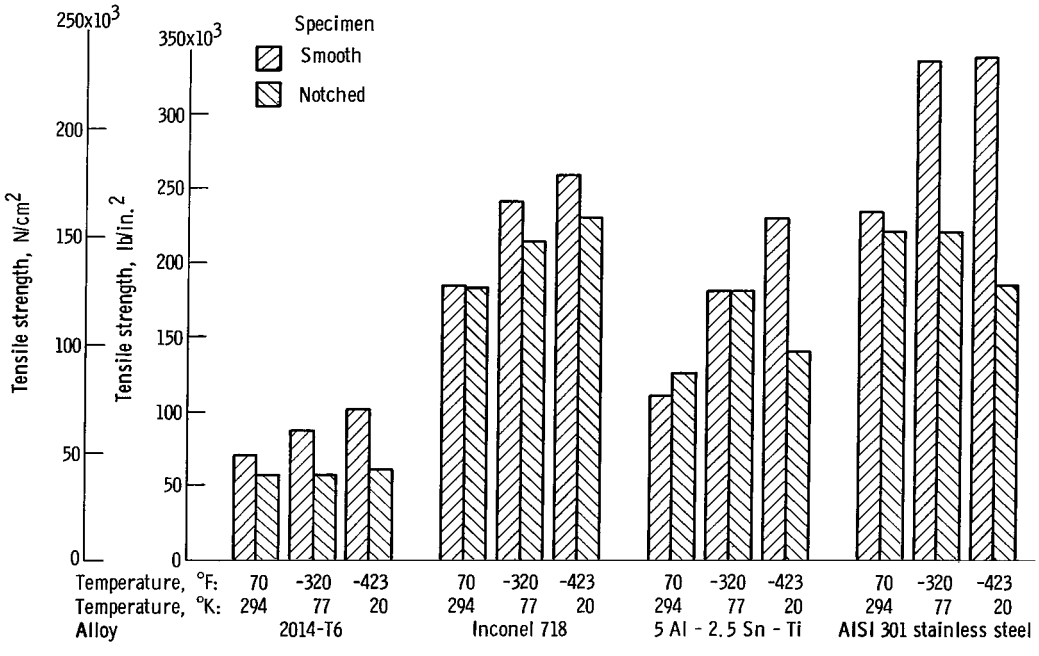

Figure 3. - Tensile strength of smooth and notched specimens of four materials as function of test temperature.

condition, Inconel 718 had notch tensile strengths that closely approached or exceeded those for notched stainless steel at cryogenic temperatures.

Stress - Cyclic-Life Relations

Fatigue curves for all the materials at all test conditions, 70° F (294° K) in ambient air, -320° F (77° K) in liquid nitrogen, and -452° F (4° K) in liquid helium, are presented in figure 4. The data points (table IV) shown at any stress level on the inclined portion of the fatigue curves represent an average of one or more individual points. In both the upper and lower horizontal portions of the fatigue curves, only individual data points are plotted.

It is interesting to consider the shape of the fatigue curves in the low-life region. In all cases there is a region of constant maximum stress that varies in length (number of cycles). The length of this portion of the fatigue curve for any material probably results from differences in tensile strength between individual specimens, and in some cases it may have been affected by work hardening due to plastic deformation during the initial loading of these specimens. These effects could also account for the instances where the maximum cyclic stress values represented by the upper horizontal portion of the fatigue curves exceed the average tensile strength values shown in figure 3 and table III.

Figure 4 shows that the fatigue strength of notched specimens in all but one case was lower than that of smooth specimens at all temperatures. The single exception was the titanium alloy which showed approximately equal fatigue strength for both smooth and notched specimens at 70° F (294° K) below 300 cycles. These results indicate that the materials were notch sensitive in fatigue as well as in tension.

For all materials, decreasing the temperature from 70° F (294° K) to -320° F (77° K) resulted in increased fatigue strength in both the unnotched and notched condition. Decreasing the temperature from -320° F (77° K) to -452° F (4° K) had different effects on fatigue strength depending on material, specimen geometry, and cyclic life. For example, for stainless steel, the fatigue strength of smooth specimens at -452° F (4° K) was, for the most part, intermediate to that obtained at 70° F (294° K) and -320° F (77° K) along the inclined portion of the fatigue curves; whereas, for notched specimens it was lowest at -452° F (4° K). The notched titanium alloy specimens also had the lowest fatigue strength at -452° F (4° K), although a crossover occurred between the 70° F (294° K) and -452° F (4° K) curves at 200 cycles.

As might be expected, Inconel 718 and 301 stainless steel generally exhibited the highest fatigue strengths and the two light metal alloys the lowest. Depending on test conditions, either Inconel 718 or 301 stainless steel had the highest fatigue lives (figs. 4(b) and (d)) when smooth specimens were considered. In the notched condition,

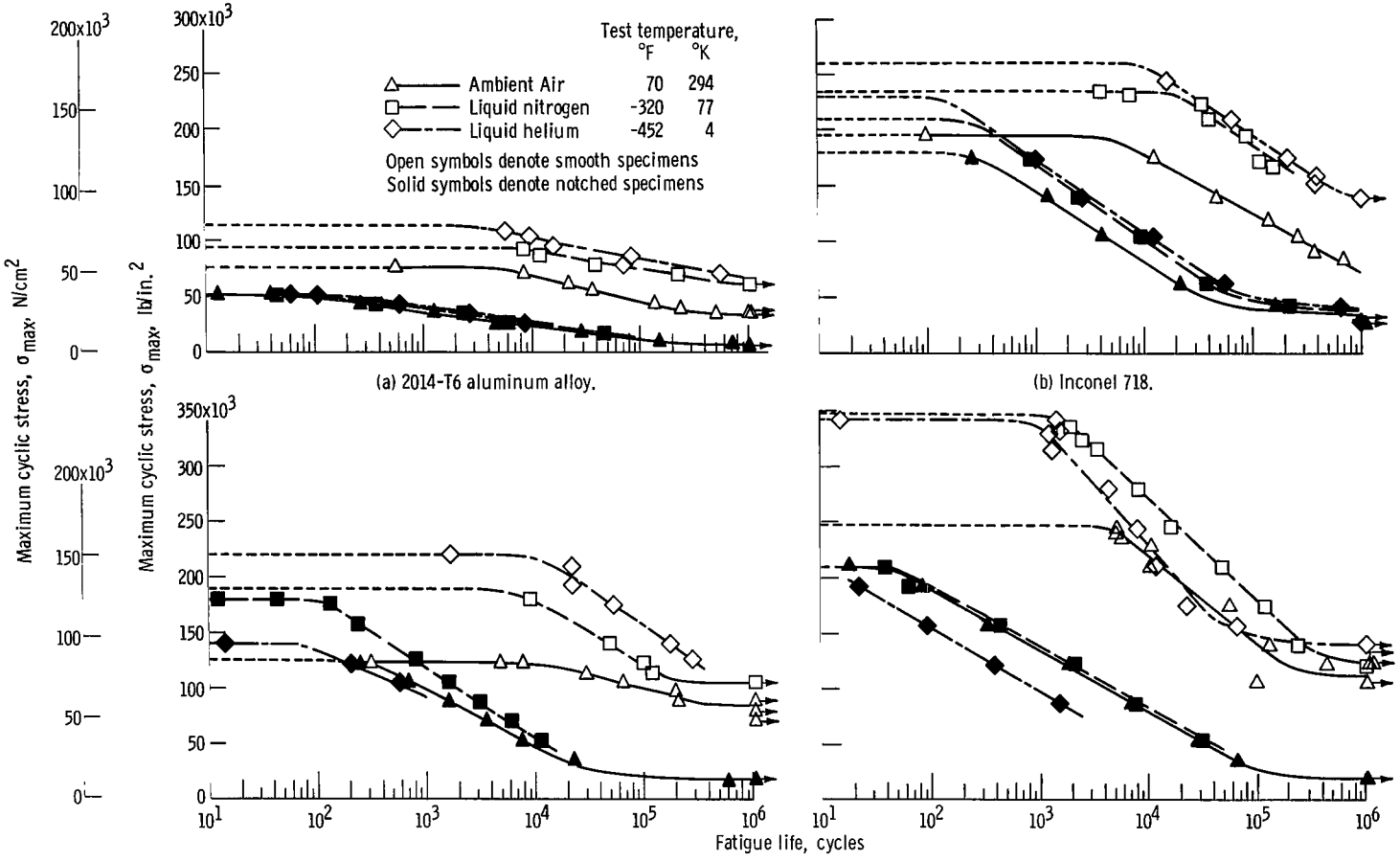

Figure 4. - Comparison of fatigue curves for smooth and notched specimens at three test temperatures. Minimum to maximum stress ratio, 0.14.

Inconel 718 generally had the highest fatigue strength of all the materials. The aluminum alloy had the lowest fatigue strengths under all conditions.

Fatigue-Strength-To-Density Relations

From the viewpoint of aerospace applications, the relative fatigue-strength-to-density ratios of the alloys is more important than simple fatigue strength. A comparison of the fatigue-strength-to-density ratios of the materials investigated at all temperatures and cyclic lives is made in figure 5. On this basis the titanium and aluminum alloys compare more favorably with the heavier nickel base and iron base alloys than on the basis of fatigue strength alone. The titanium alloy, when tested in the unnotched condition, was consistently stronger than the other three materials over a major part of the cyclic life range. In the notched condition, however, the fatigue-strength-to-density ratio of this alloy tended to decrease with decreasing applied stress so that for longer test times (10^4 cycles and up at 70° F (294° K) and -320° F (77° K)) this alloy was not as strong as some of the other materials. Inconel 718, on the other hand, was one of the poorer materials in the unnotched condition, but in the notched condition, especially for longer test lives, it was generally the best material at all temperatures.

Notch Effects

It has already been pointed out that all the materials considered were generally notch sensitive in fatigue. The degree of notch sensitivity over the entire cyclic life range and at all test temperatures is illustrated in figure 6. In figure 6, the fatigue notch factor (ratio of smooth specimen fatigue strength to notched specimen fatigue strength for any single life value), is plotted against cyclic life for each material. The tensile notch factor (ratio of smooth specimen tensile strength to notched specimen tensile strength) is plotted at 1/2 cycle. The form of the fatigue notch factor K_f curves of figure 6 resulted from the relative positions with respect to each other of the unnotched and notched material fatigue curves of figure 4. In considering these curves, it should be recognized that the specimen geometry has a direct bearing on the numerical values for fatigue notch factor. The values would undoubtedly have been different for other specimen geometries. It is believed, however, that the basic trends shown would be the same regardless of geometry.

Figure 6 shows that, up to approximately 50 to 100 cycles, the fatigue notch factor was nearly the same as the tensile notch factor for the respective materials at all temperatures. As cyclic life increased, however, the fatigue notch factor also increased. In those instances where data were obtained up to and beyond 10^5 cycles, the trend of

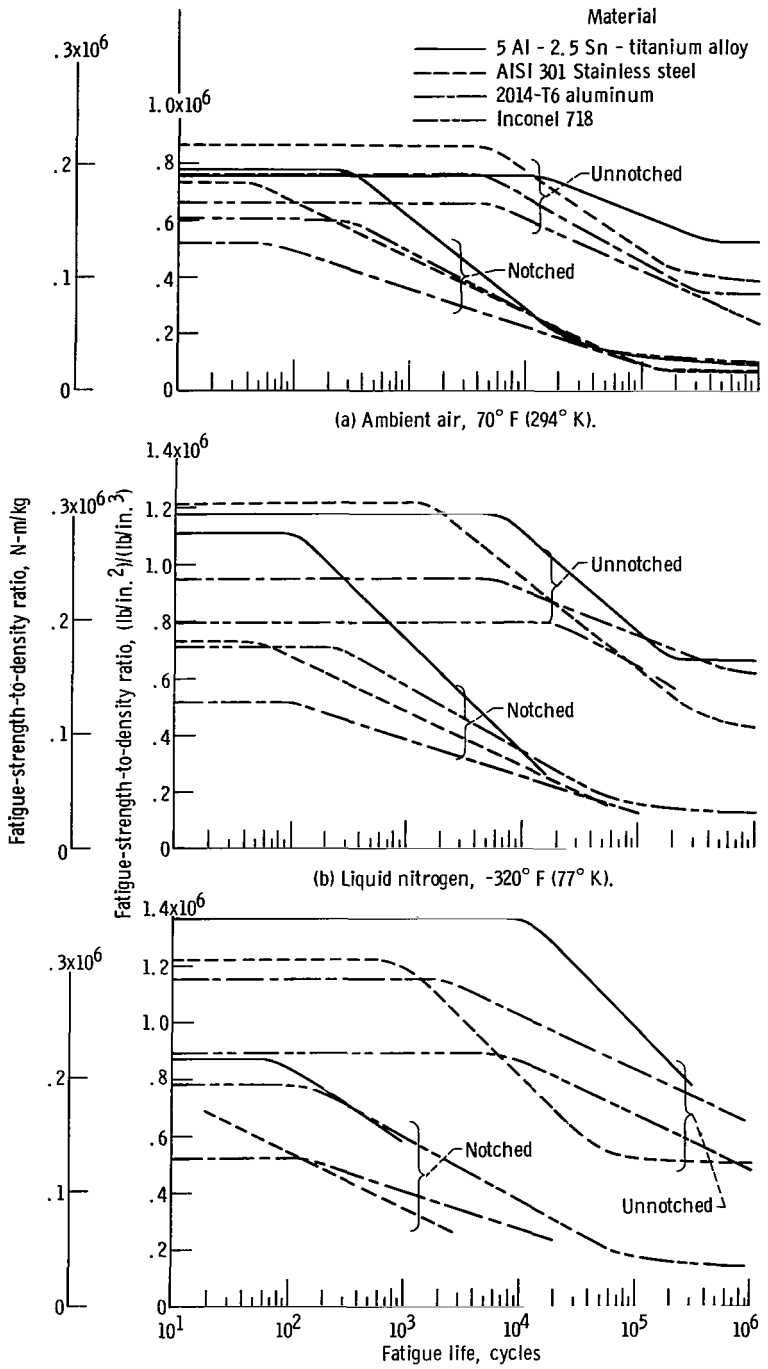

(a) Ambient air, 70° F (294° K).

(b) Liquid nitrogen, -320° F (77° K).

(c) Liquid helium, -452° F (4° K).

Figure 5. - Comparison of fatigue-strength-to-density ratios of four materials at three test temperatures.

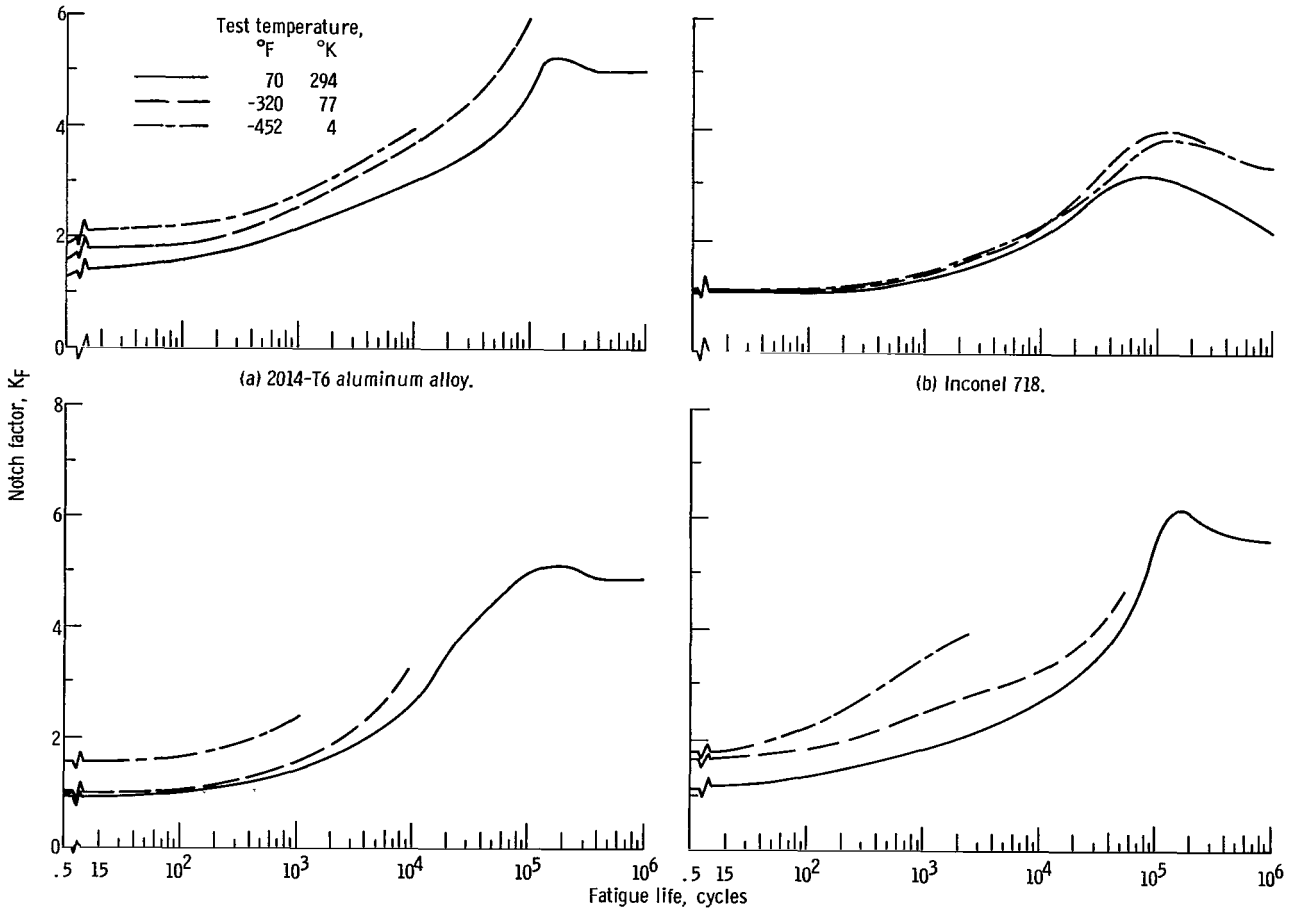

Figure 6. - Variation of fatigue notch factor with testing temperature and fatigue life. Minimum to maximum stress ratio, 0.14.

increasing fatigue notch factor with increasing fatigue life was either halted or reversed at approximately 10^5 cycles.

Inconel 718 generally had the lowest fatigue notch factors at all test temperatures over the life range considered. The aluminum alloy had slightly higher notch factors than either the titanium alloy or the stainless steel at low cyclic lives. Although sufficient data are not available to determine the notch factor up to 10^5 cycles at -452° F (4° K) and at -320° F (77° K) for either the titanium alloy or the stainless steel and at -452° F (4° K) for the aluminum alloy, it appears from extrapolation that a fairly steep rise in notch factor would probably occur beyond the cyclic life values where these curves were terminated. It is evident from the comparisons of figure 6 that the presence of a notch can drastically affect the permissible operating stress at all temperatures. At higher cyclic lives the fatigue notch factor can be many times greater than the tensile notch factor, and tensile data are not adequate for anticipating the effect of stress concentrations under fatigue loading.

Figure 6 also shows that the fatigue notch factor increased progressively with decreasing temperature for all materials except Inconel 718. In this alloy it was virtually the same at all temperatures up to approximately 4×10^4 cycles. At higher cyclic lives, an appreciable spread in the fatigue notch factor curves is evident for this material.

Relation Between Tensile and Fatigue Data

It was pointed out in reference 26 that at room temperature the fatigue life of 1/4-inch- (0.64-cm-) diameter smooth specimens of a large variety of materials is functionally related to their tensile properties under the condition of reversed, symmetric cyclic strain. An attempt was made to determine whether or not analogous relations could be applied to the axial-tensile fatigue life data generated in this investigation, wherein the load range rather than the strain range was specified. The elastic strain ranges established by the load ranges applied were therefore determined. According to reference 26, the elastic strain range for a smooth specimen can be determined from tensile properties by use of the following equation:

$$\Delta\epsilon_{el} = \frac{3.5\,\sigma_u}{E} N^{-0.12} \text{ (Smooth specimen)} \tag{1}$$

where

$\Delta\epsilon_{el}$ elastic strain range

σ_u ultimate tensile strength

E modulus of elasticity

N number of cycles to failure

Equation (1) was used to establish the positions of the lines that describe smooth specimen fatigue behavior in figure 7. The experimental values of elastic strain range $\Delta\epsilon_{el}$, plotted against experimental life values in figure 7 for both the smooth and notched specimens, were calculated from the expression

$$\Delta\epsilon_{el} = \frac{\sigma_{max}}{E} \tag{2}$$

where σ_{max} is the nominal maximum cyclic tensile stress (load divided by original

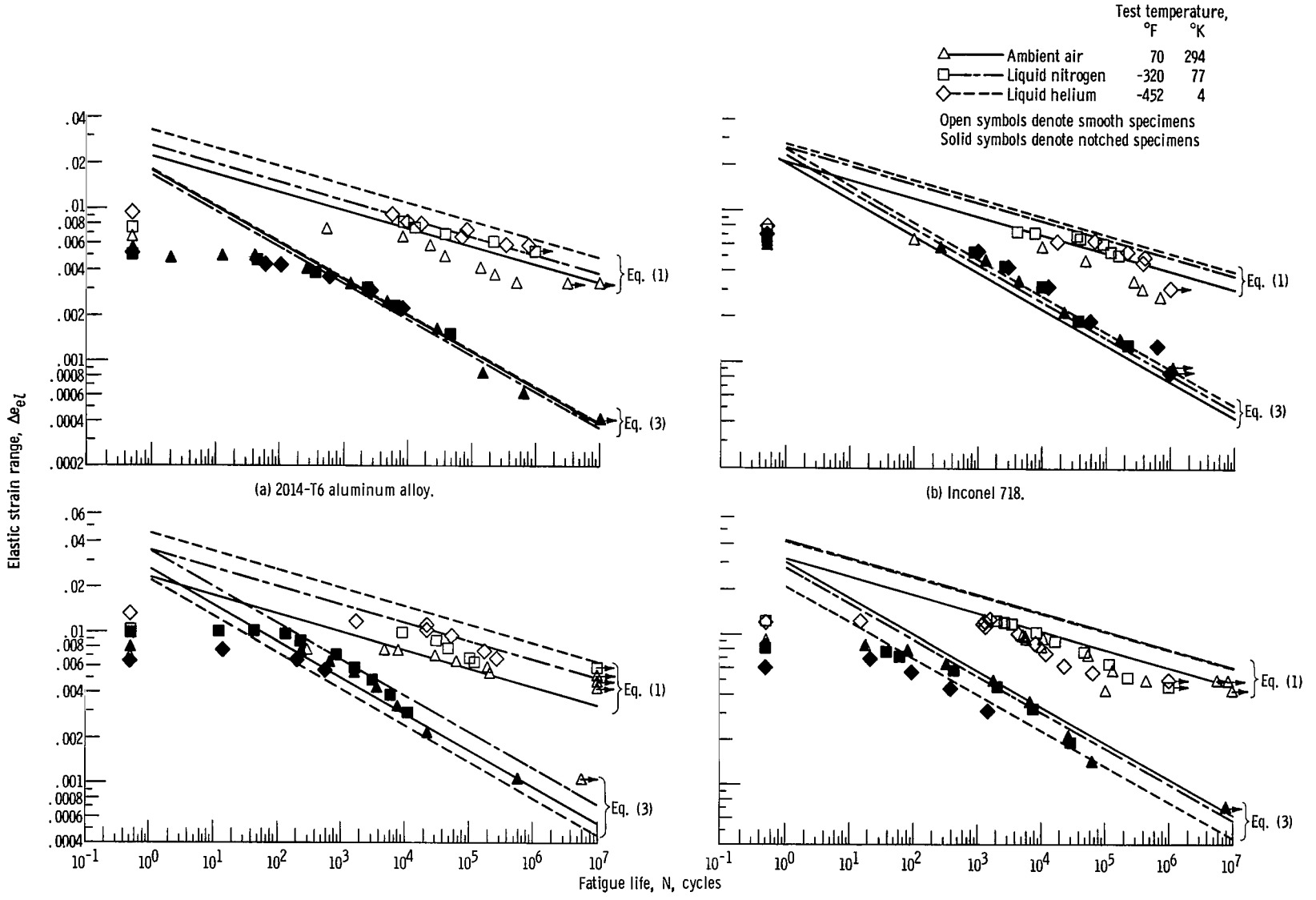

(a) 2014-T6 aluminum alloy.

(b) Inconel 718.

(c) 5 Al - 2.5 Sn - titanium alloy.

(d) AISI 301 Stainless steel.

Figure 7. - Relations between elastic strain range and fatigue life for smooth and notched specimens at three test temperatures.

cross sectional area). Use of this expression assumed that cyclic stress range ($\sigma_{max} - \sigma_{min}$) could reasonably be approximated by the maximum cyclic stress applied in each test.

Comparison of the smooth specimen data and the lives predicted by equation (1) indicated the equation to be valid, at least above 1000 cycles, for the condition of the present investigation where the mean tensile stress was greater than zero. Figure 7 also indicates that equation (1) was not valid for notched specimens. However, a relation similar to that of equation (1) reasonably approximates the data. This relation is expressed as

$$\Delta\epsilon_{el} = \frac{3.5\,\sigma_u}{E} N^{-0.24} \text{ (Notched specimen)} \qquad (3)$$

Several factors favor the use of equations (1) and (3) as a reasonable approximation of fatigue behavior under the conditions of test considered in this investigation:

(1) The fatigue life-strain range relations are correct to within approximately the temperature-induced bandwidth established by the tensile data.

(2) The temperature-induced changes in tensile properties are reflected in the temperature dependence of fatigue life for each material, and temperature separations in the curves and fatigue data are usually of the same order for a given material.

(3) Pronounced deviations between experimental data and the curves represented by equations (1) and (3) occur only in the range of short-life tests. These probably arise because the plastic component of strain was not taken into account.

(4) The comparison of the lines defined by equations (1) and (3) with the experimental data for all the materials emphasizes that some functional relation between tensile and fatigue data exists at cryogenic temperatures and, further, suggests that structural changes induced by tensile loading may be related to those induced by fatigue loading.

Metallography

Macrographs and micrographs of the materials investigated are presented in figures 8 to 27. Etchants used are listed in table V. The results of the metallographic investigation of each material are discussed in the following sections.

2014 T-6 Aluminum alloy. - Macrographs of failed tensile specimens of 2014-T6 aluminum alloy tested at 70° F (294° K), -320° F (77° K), and -423° F (20° K) that show characteristic fracture modes and relative elongations are presented in figure 8. The increase in elongation with decreasing test temperature, although small, is observable. The fracture mode was similar regardless of temperature. No pronounced necking occurred. Although not evident from the macrograph, the fracture surface is on a plane

TABLE V. - ETCHANTS USED ON SPECIMENS

Material	Etchant	
	Desig-nation	Composition
2014-T6 aluminum alloy	A	30 ml glycerine, 20 ml nitric acid, 10 ml hydrofluoric acid
	B	5 g sodium hydroxide, 5 g sodium carbonate, 100 ml water
Inconel 718	C	30 ml hydrochloric acid, 30 ml lactic acid, 10 ml nitric acid, 10 g cuprous chloride
5Al-2. 5Sn-Ti alloy	D	30 ml glycerine, 10 ml nitric acid, 10 ml hydrofluoric acid, 50 ml water
AISI 301 Stainless steel	E	10 percent oxalic acid electrolytic etchant followed by swab in 30 percent nitric acid - 20 percent acetic acid solution

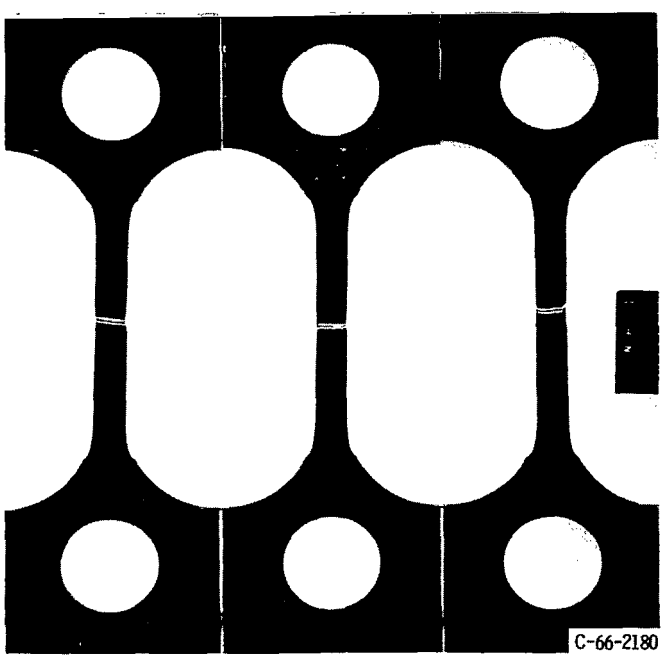

(a) 70° F (294° K). (b) -320° F (77° K). (c) -423° F (20° K).

Figure 8. - Macrophotographs of failed 2014-T6 aluminum alloy tensile specimens showing characteristic fracture modes and final elongations for three test temperatures.

inclined approximately 45° to the plane of the specimen.

The microstructure of the as-received material is shown in figure 9 at two magnifications. Two different etchants were used to delineate the microstructural features. Numerous minor phase particles are evident throughout the alloy matrix. A microetching technique (ref. 27) was used to identify the light gray particles as an aluminum (Al)-copper (Cu)-iron (Fe)-manganese (Mn) intermetallic. An electron microprobe analysis indicated that they also contained silicon. The same microetching technique showed that the dark gray particles were Al-Cu-nickel (Ni) intermetallics, although the alloy con-

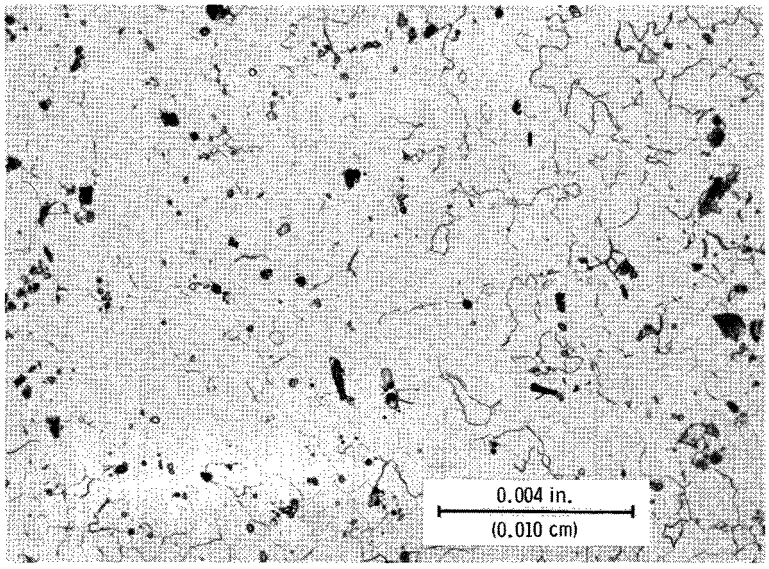

(a) Etchant A.

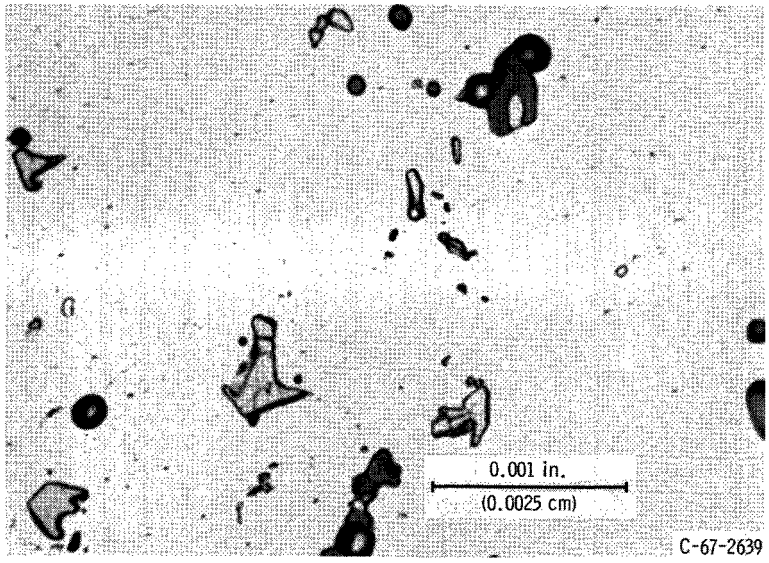

(b) Etchant B.

Figure 9. - Microstructure of as-received 2014-T6 aluminum alloy sheet.

tained only 0.009 percent nickel. Electron microprobe analyses were used to identify the black particles (usually spherical and often associated with the dark gray ones) as an Al-$CuAl_2$ eutectic.

It is evident from figures 10 and 11 that the light particles (Al-Cu-Fe-Mn-silicon (Si)) are susceptible to cracking during the fatigue test. Micrographs of notched fatigue specimens tested at three different stress levels at room temperature are shown in figure 10. The number of minor phase particles that cracked increased with increasing stress. No cracked particles appear in the specimen tested below the fatigue limit (fig. 10(a)); however, in specimens tested at higher stresses, many such cracked particles are seen in the region adjacent to the fracture path (fig. 10(c)). A similar trend was observed at all temperatures, but the "threshold stress" below which no particle cracking was observed was progressively higher as the test temperature decreased. Figure 11 shows the effect of the minor phase particles on the fatigue failure mode. The similarity of the fracture mode in notched specimens cycled at the same stress but at three different temperatures is apparent. Tests of all specimens shown in figure 11 were terminated prior to complete separation so as to observe the fracture mode more clearly. The cracks emanating from the notch root are shown. In each instance the gray minor phase particles are linked by the main crack giving it a jagged, irregular appearance. Particles adjacent to the main fracture path are also cracked. It is believed that the minor particles were cracked when the region was plastically deformed during the test and that cracks emanating from the notch root progressed from one cracked particle to another and passed through them. Thus, each cracked particle can be considered as a microscopic area of weakness. Another investigator (ref. 28) observed by electron microscopy that constituent particles in the matrix of two aluminum alloys cracked or cleaved in a similarly brittle fashion. He also showed that the microscopic crack growth rate through the particles was higher than it was through the alloy matrix. It should be noted that in the present investigation particle cracking was confined to the gray phase (Al-Cu-Fe-Mn-Si). When the main crack encountered the darker minor phase particles (either the Al-Cu-Ni or Al-$CuAl_2$), it tended to circumvent them, which suggests that these phases may be beneficial insofar as fatigue crack resistance is concerned in this alloy.

Inconel 718. - The macrographs of failed tensile specimens of Inconel 718 (fig. 12) indicate the fracture mode to be somewhat similar to that of the 2014 T-6 aluminum alloy. Only specimens tested at room temperature showed an observable amount of necking in the fracture area. A noticeable increase in total elongation over that obtained at room temperature is evident at both -320° F (77° K) and -423° F (20° K). All specimens had an orange-peel texture in the test section, but this was more pronounced and extended over a greater length for the specimens tested at the cryogenic temperatures.

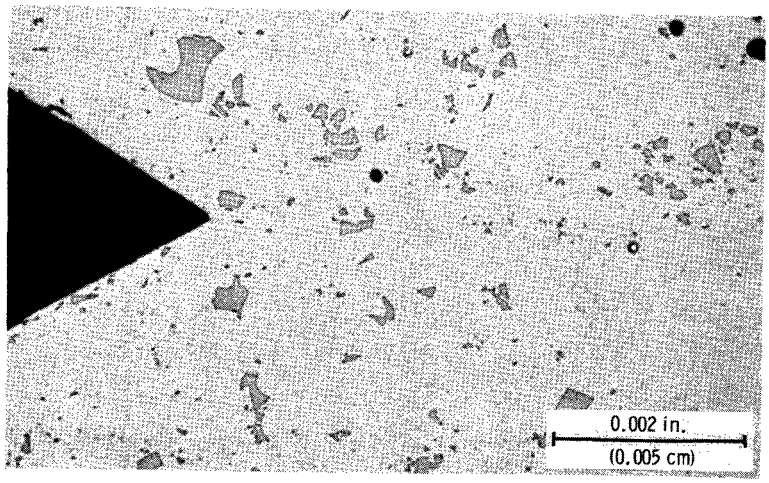

(a) 11 200 000 Cycles at maximum stress of 4380 pounds per square inch (3000 N/cm^2).

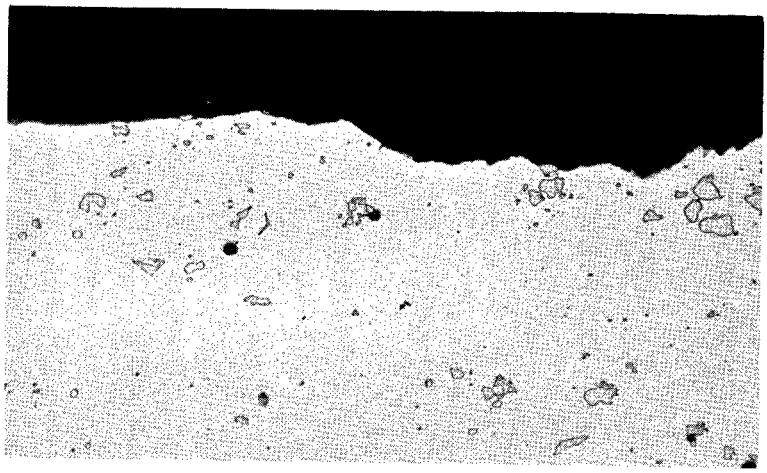

(b) 615 000 Cycles at maximum stress of 6520 pounds per square inch (4500 N/cm^2).

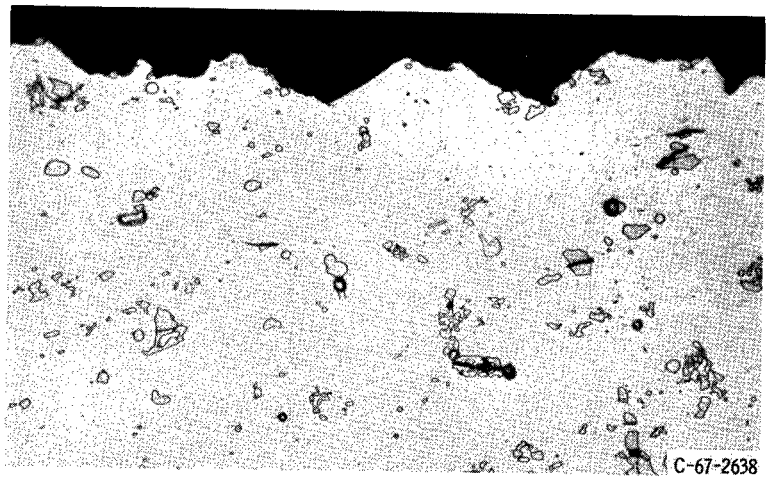

(c) 230 Cycles at maximum stress of 43 750 pounds per square inch (30 200 N/cm^2).

Figure 10. - Photomicrographs illustrating increased degree of minor phase cracking caused by increased stress in notched 2014-T6 aluminum fatigue specimens at room temperature. Etchant B.

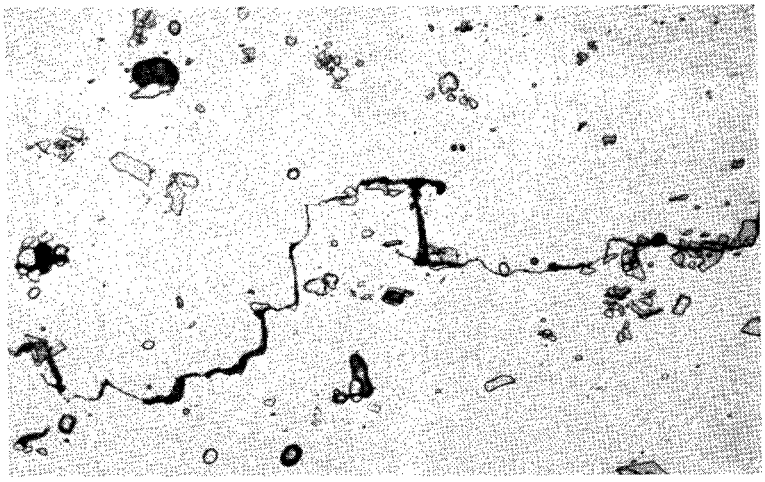

(a) Test temperature, -452° F (4° K); ratio of cycles applied to cycles to fracture, 0.4.

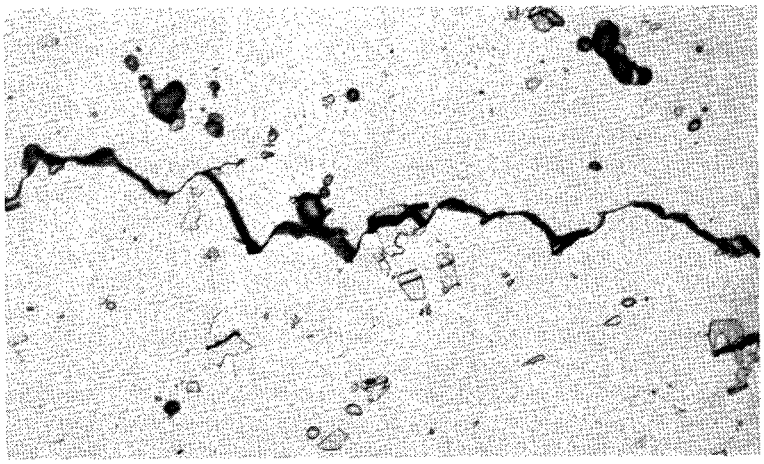

(b) Test temperature, -320° F (77° K); ratio of cycles applied to cycles to fracture, 0.5.

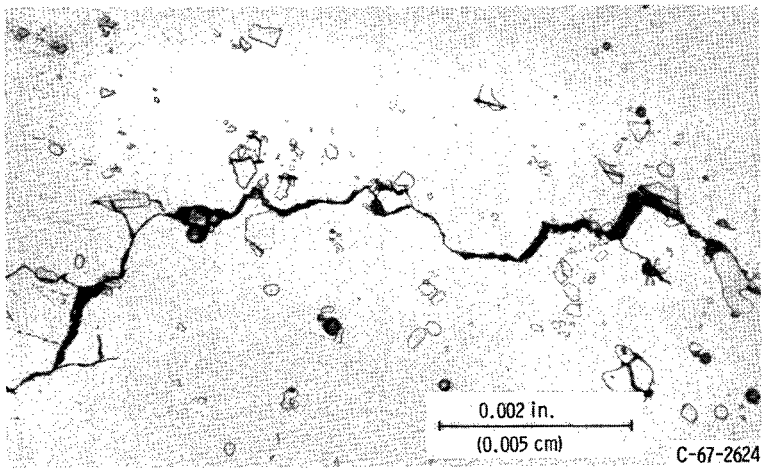

(c) Test temperature, 70° F (294° K); ratio of cycles applied to cycles to fracture, 0.8.

Figure 11. - Photomicrographs illustrating fatigue fracture mode in 2014-T6 aluminum alloy. Main crack passes through and links cracked minor phase particles. Notched specimens removed from test after 1000 cycles at 35 000 pounds per square inch (24 130 N/cm^2). Etchant B.

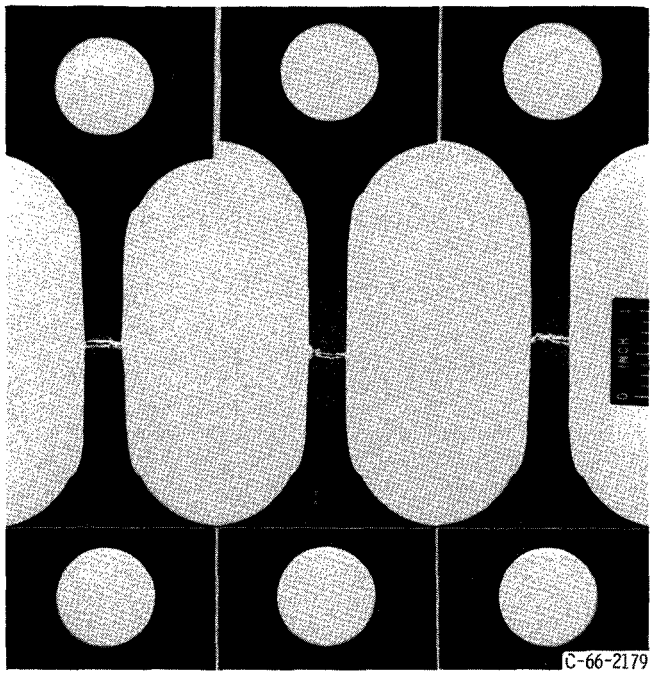

(a) 70° F (294° K). (b) -320° F (77° K). (c) -423° F (20° K).

Figure 12. - Macrophotographs of failed Inconel 718 alloy tensile specimens showing characteristic fracture modes and final elongations for three test temperatures.

A duplex grain structure was observed in the Inconel 718 material. Figure 13 shows micrographs of both mill-annealed (as-received) and solution-treated microspecimens. The micrographs of the solution-treated material were taken from the same microspecimen but show opposite surfaces of the original 0.093-inch- (2.36-mm) thick sheet. It was noted that the average grain size of the solution-treated sample was greater than that of the mill-annealed sample but that a duplex grain structure was still present.

Figure 14 illustrates the microstructure in the region adjacent to the fracture surface of notched fatigue specimens tested at a maximum cyclic stress of 175 000 pounds per square inch (120 600 N/cm^2). All three test temperatures are represented. Considerable cracking of minor phase particles occurred in this material; however, unlike 2014-T6 aluminum alloy, the main fracture path does not preferentially pass through these particles. This fracture path may be observed more clearly in figure 15, which shows the microstructure of Inconel 718 notched fatigue specimens tested at 105 000 pounds per square inch (72 400 N/cm^2). In this case, the specimens were removed from the test prior to complete separation to observe the fracture mode better. The mode of fracture was clearly transgranular at all temperatures. The minor phase particles did not crack at this particular stress level, and the main fracture path appears to go around them rather than through them. Deformation bands are evident in the immediate vicinity of the crack, which seems to follow along these slip bands; this is particularly apparent

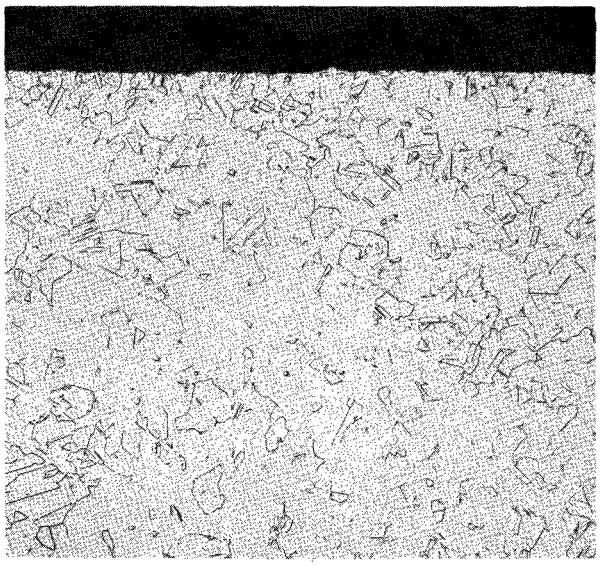

(a) As-received.

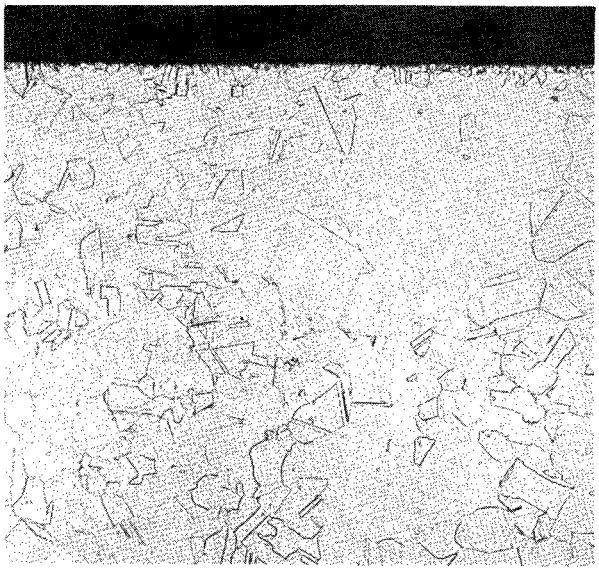

(b) Solution heat-treated 1 hour at 1950° F (1339° K). One surface of specimen.

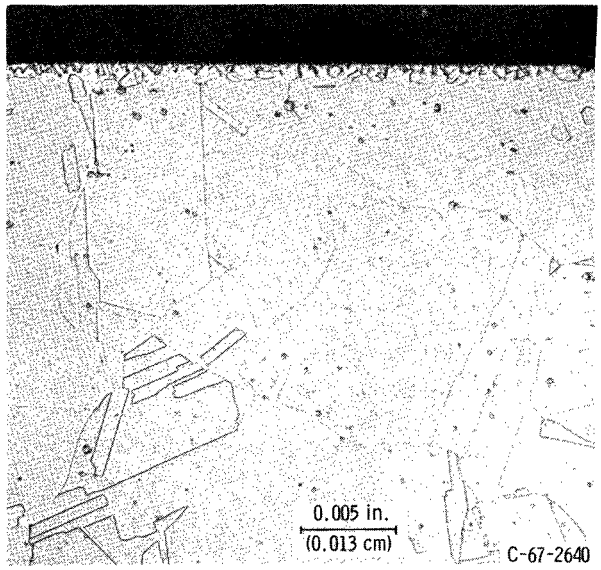

(c) Solution heat-treated 1 hour at 1950° F (1339° K). Opposite surface of specimen.

Figure 13. - Photomicrograph of Inconel 718 specimens. Etchant C.

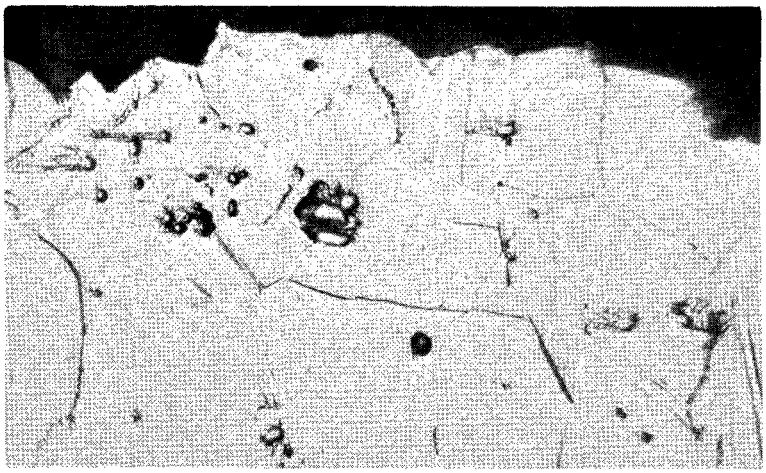

(a) Test temperature, -452° F (4° K).

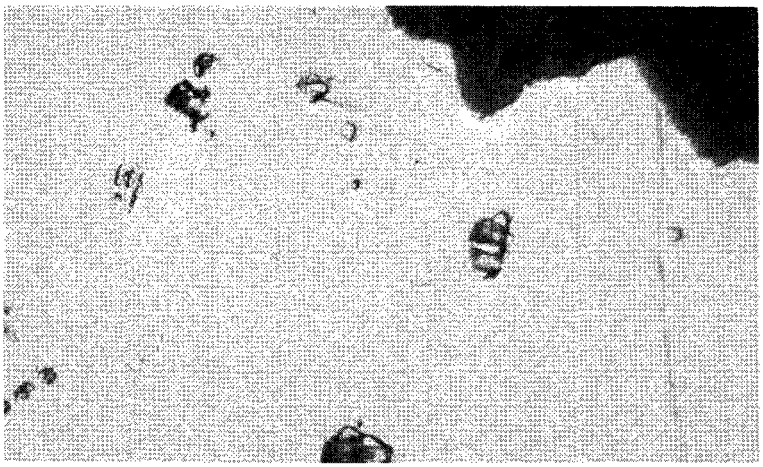

(b) Test temperature, -320° F (77° K).

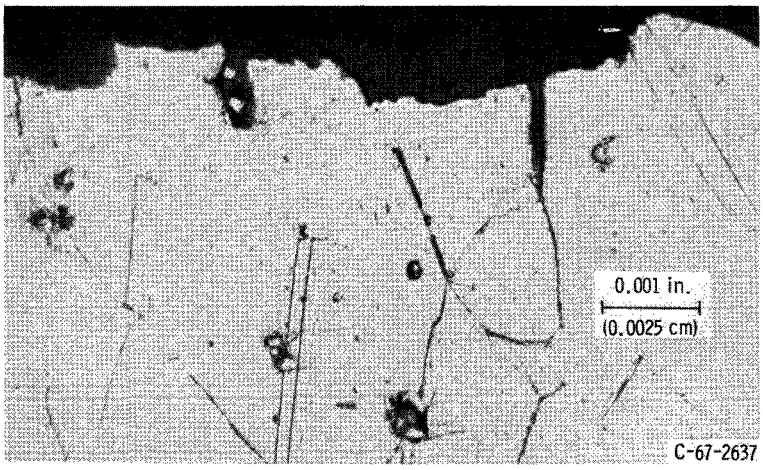

(c) Test temperature, 70° F (294° K).

Figure 14. - Zones immediately adjacent to fracture surfaces of notched Inconel 718 fatigue specimens tested at relatively high maximum cyclic stress of 175 000 pounds per square inch (120 600 N/cm^2) showing cracked particles, but no linking of cracked particles by crack that caused fracture. Etchant C.

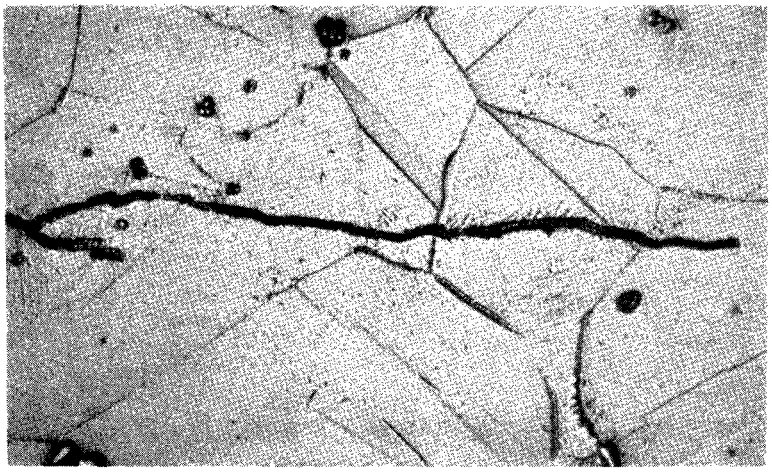

(a) Test temperature, -452° F (4° K); ratio of cycles applied to cycles to fracture, 0.3.

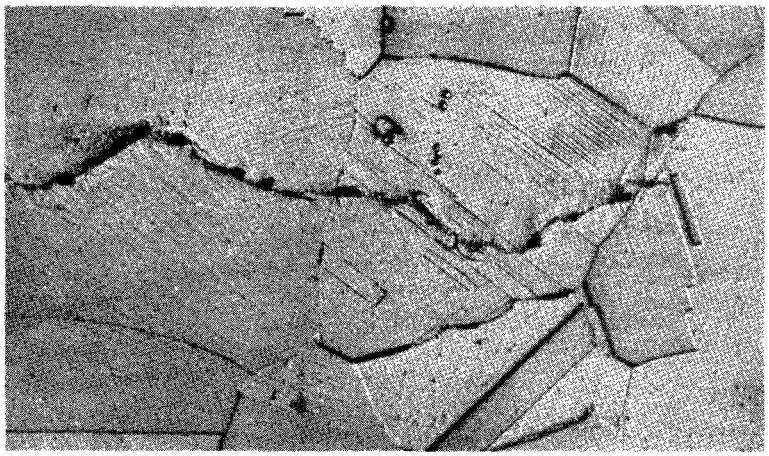

(b) Test temperature, -320° F (77° K); ratio of cycles applied to cycles to fracture, 0.4.

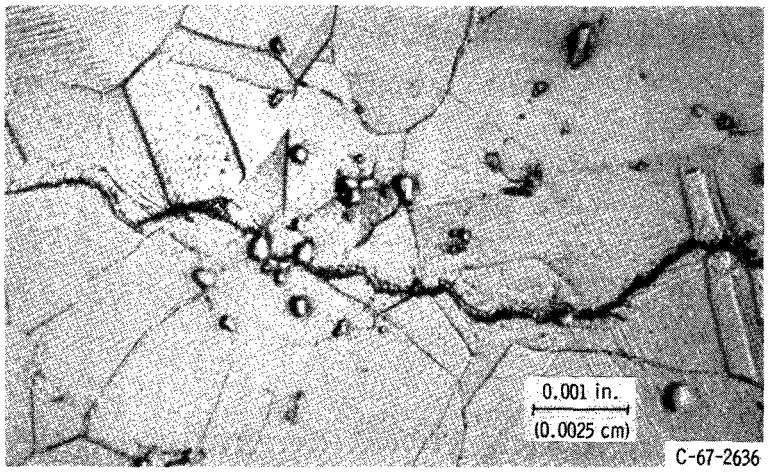

(c) Test temperature, 70° F (294° K); ratio of cycles applied to cycles to fracture, 0.8.

Figure 15. - Fatigue cracks in notched Inconel 718 specimens tested at relatively low maximum cyclic stress of 105 000 pounds per square inch (72 400 N/cm^2). No evidence of minor phase cracking; main crack follows along slip planes and around minor phase particles; tests stopped at 3500 cycles, before specimens failed. Etchant C.

for the specimen tested at -320° F (77° K).

5Al-2.5Sn-Ti alloy. - Macrographs of failed tensile specimens of the 5Al-2.5Sn-titanium alloy (fig. 16) illustrate several interesting features. Unlike either the aluminum or the nickel alloy, there was considerable localized necking in the fracture region of specimens tested at both room temperature and -320° F (77° K). In specimens tested at -423° F (20° K), there was little or no necking in the test section. Also, the fracture surface was smooth, clearly different from the jagged fracture surface caused by testing at 70° F (294° K) and the jagged, V-shaped fracture surface observed after testing at -320° F (77° K). The plane of fracture in all cases was normal to the plane of the sheet specimen. Elongation decreased slightly in progressive fashion with decreasing test temperature. From the macrographs it would appear that a different mechanism controls failure at -423° F (20° K) than at the other test temperatures.

The microstructure of the as-received alloy is shown in figure 17. The grains are equiaxed and fairly uniform in size. Smooth tensile specimen micrographs, taken in the region about 1/4 inch (6.4 mm) away from the fracture area, are shown in figure 18. At room temperature the grains were considerably deformed in the direction of the test stress with no observable twinning. At -320° F (77° K) there was still considerable elongation of the grains and twins are evident in only a few grains. At -423° F (20° K), however, the primary mode of deformation was by twinning and the grains remained equiaxed. For notched tensile-tested specimens (fig. 19) the microstructures show that twinning occurred at all test temperatures with the greatest amount of twinning occurring at -423° F (20° K). Also, the grains appear to be equiaxed at all temperatures.

Micrographs of smooth and notched fatigue-tested specimens are presented in figures 20 and 21, respectively. Figure 20 shows the microstructure in areas about 1/4 inch (6.4 mm) from the fracture surface for smooth specimens operated to failure in approximately 30 000 cycles. The required stress level to obtain this cyclic life increased with decreasing temperature. Pronounced twinning was evident at -452° F (4° K), and some was also evident at -320° F (77° K) but none at room temperature. Figure 21 shows micrographs of notched fatigue specimens that were removed from the test prior to complete separation to observe the fracture mode better. All specimens were run for 400 cycles at a maximum stress of 105 000 pounds per square inch (72 400 N/cm^2). Polarized light was used in obtaining the photomicrographs to illustrate the shape of twins. The crack tip is identified by the arrows. As in the case of notched tensile specimens, twins occurred at all test temperatures and in this case were as pronounced at room temperature as at -452° F (4° K). The relatively small number of twins evident at -320° F (77° K) is possibly due to the fact that the crack length (upper righthand corner) when the test was stopped was considerably less than that at the conclusion of tests at each of the other temperatures. Since all three specimens were subjected to the same load, the shorter crack length in the specimen tested at -320° F (77° K) resulted in a lower net

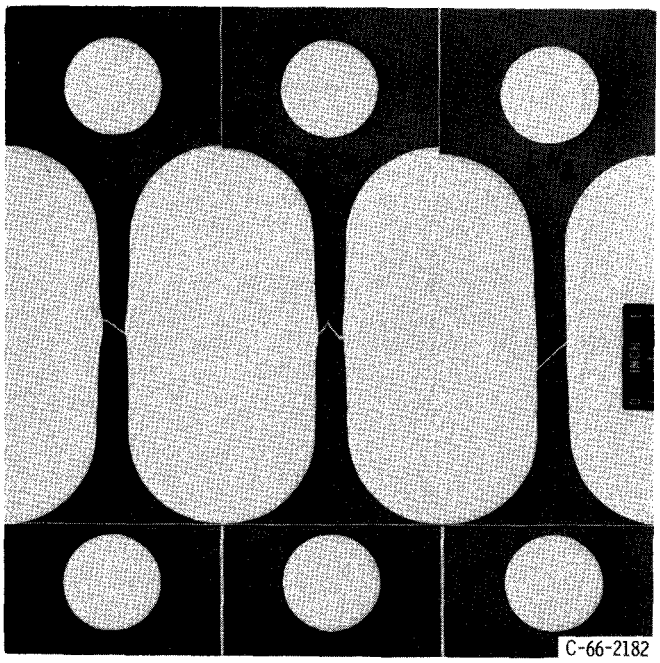

(a) 70° F (294° K). (b) -320° F (77° K). (c) -423° F (20° K).

Figure 16. - Macrophotographs of failed 5 Al- 2.5 Sn-Ti alloy tensile specimens showing characteristic fracture modes and final elongations for three test temperatures.

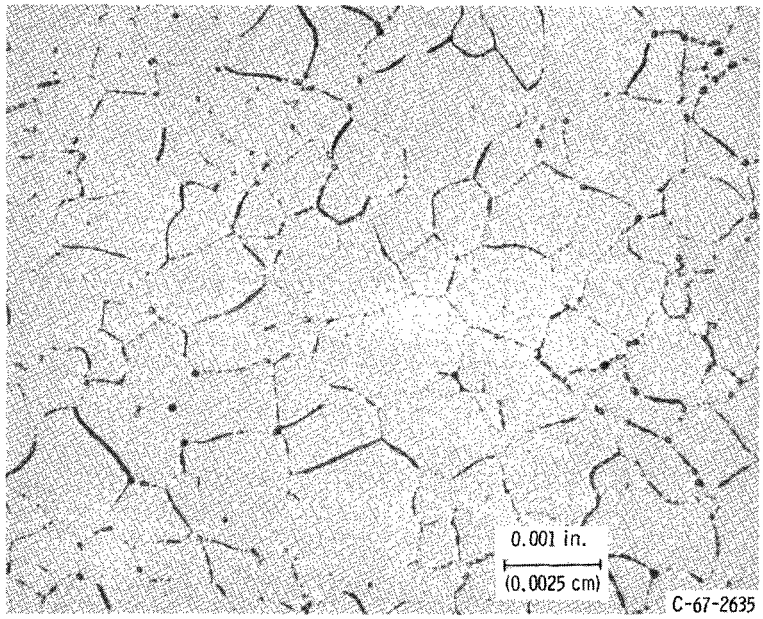

Figure 17. - Microstructure of as-received 5 Al- 2.5 Sn-Ti alloy sheet. Etchant D.

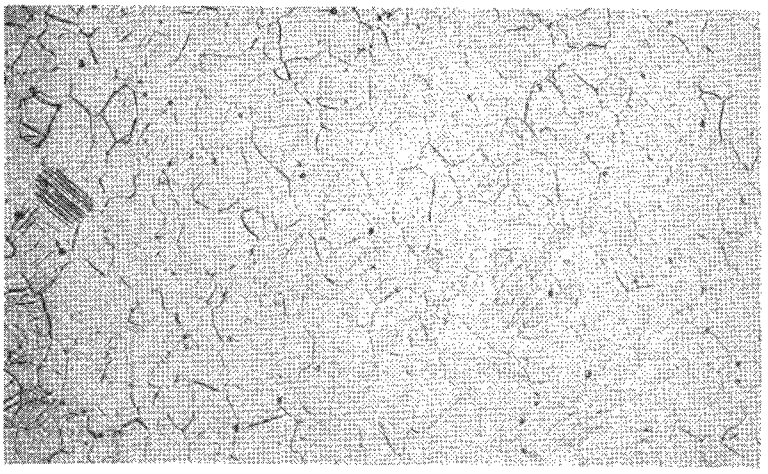

(a) -423° F (20° K).

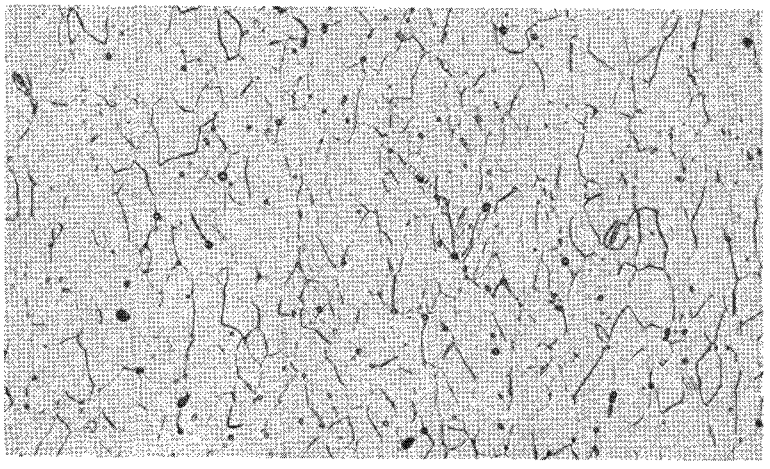

(b) -320° F (77° K).

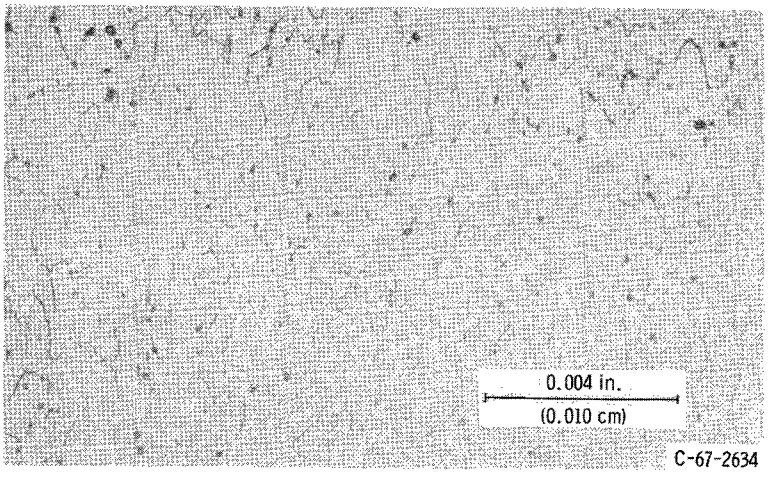

(c) 70° F (294° K).

Figure 18. - Photomicrographs of 5 Al -2.5 Sn-Ti alloy smooth tensile specimens, showing progressive decrease in grain elongation and increased number of twins as test temperature was lowered. Areas shown approximately 1/4 inch (6.4 mm) from fracture surface; loading axis vertical; etchant D.

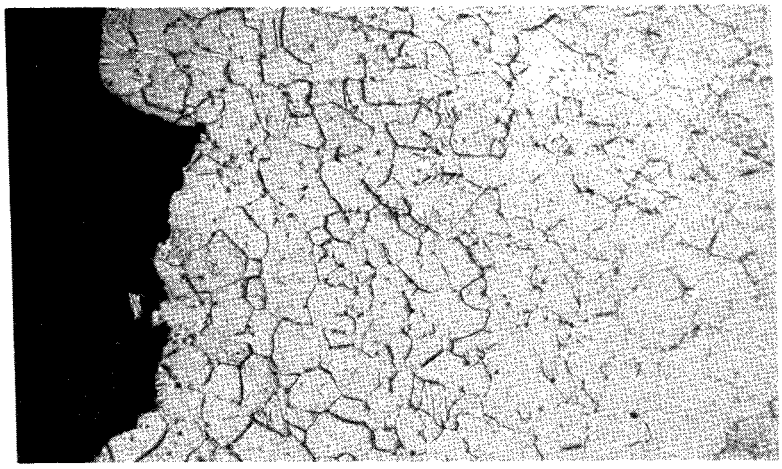

(a) -423° F (20° K).

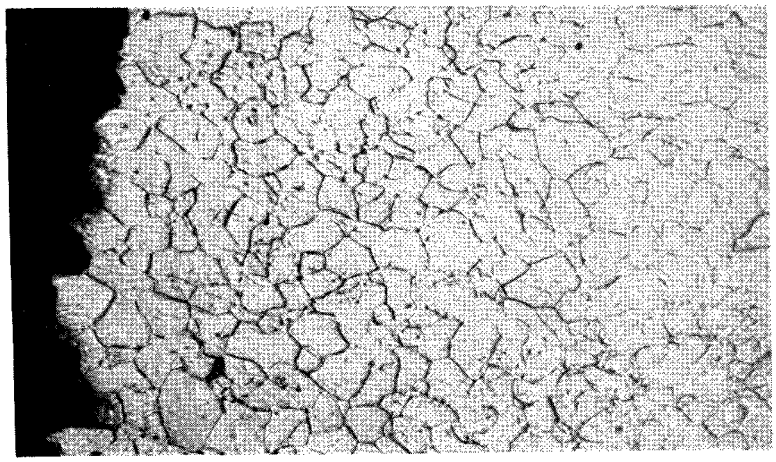

(b) -320° F (77° K).

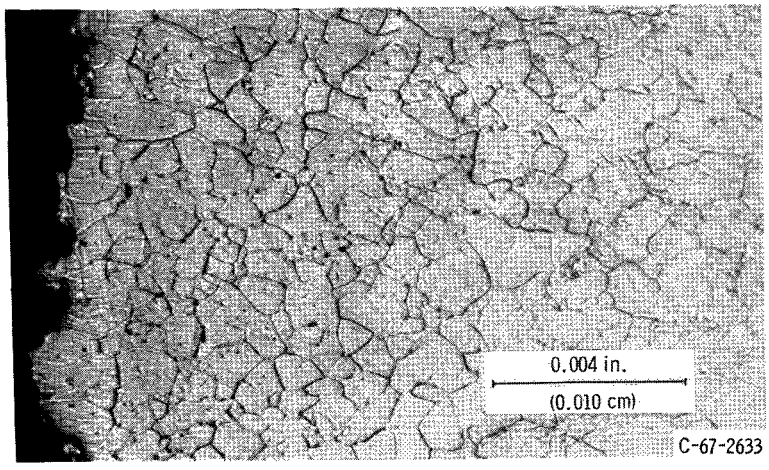

(c) 70° F (294° K).

Figure 19. - Photomicrograph of 5 Al -2.5 Sn-Ti notched tensile specimens showing equiaxed grains at all test temperatures. Relatively few twins occurred at 70° F (294° K) and -320° F (77° K) and many twins at -423° F (20° K). Etchant D.

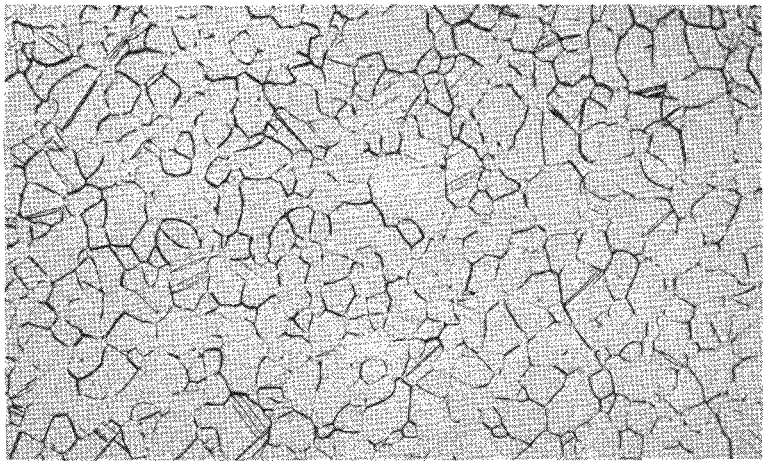

(a) -452° F (4° K); stress, 192 500 pounds per square inch (132 700 N/cm^2); life, 29 200 cycles.

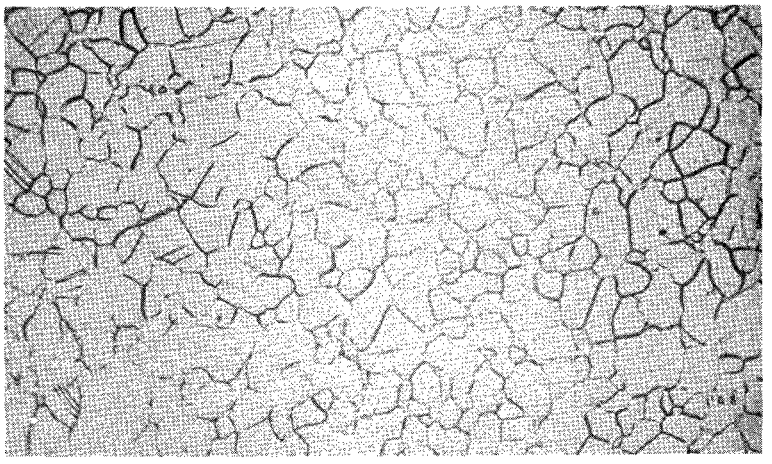

(b) -320° F (77° K); stress, 157 500 pounds per square inch (108 600 N/cm^2); life, 30 800 cycles.

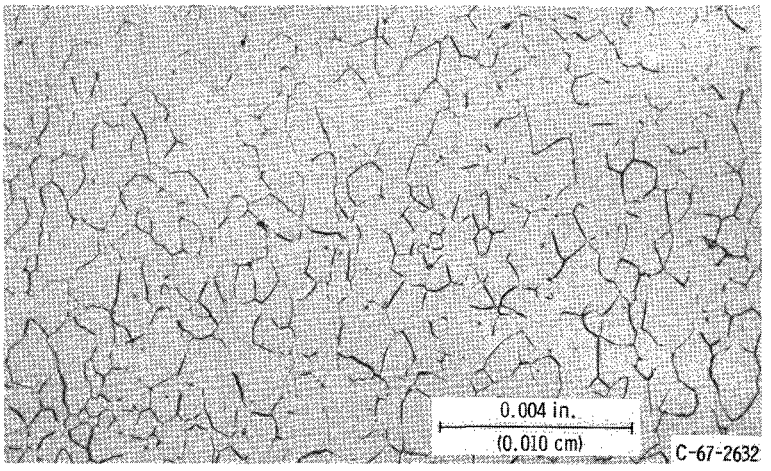

(c) 70° F (294° K); stress, 114 000 pounds per square inch (78 500 N/cm^2); life, 29 700 cycles.

Figure 20. - Photomicrographs of smooth 5 Al -2.5 Sn-Ti alloy fatigue specimens showing progressive decrease in grain elongation and increase in twinning as test temperature was reduced. Areas shown 1/4 inch (6.4 mm) from fracture surface; loading axis vertical; etchant D.

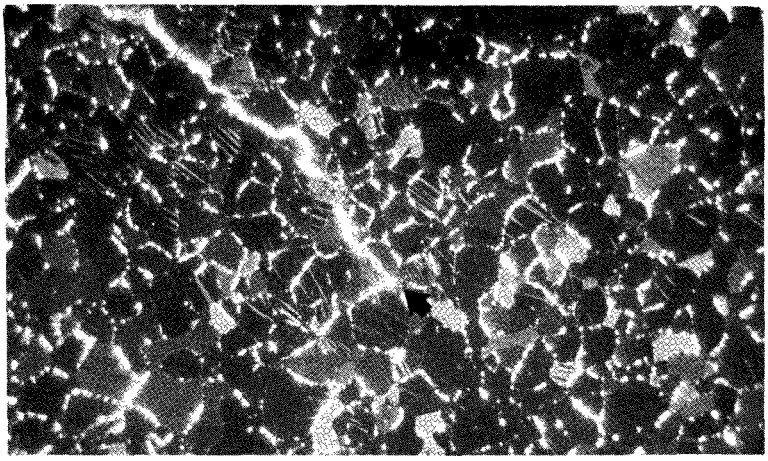

(a) Test temperature, -452° F (4° K); ratio of cycles applied to cycles to fracture, 0.7.

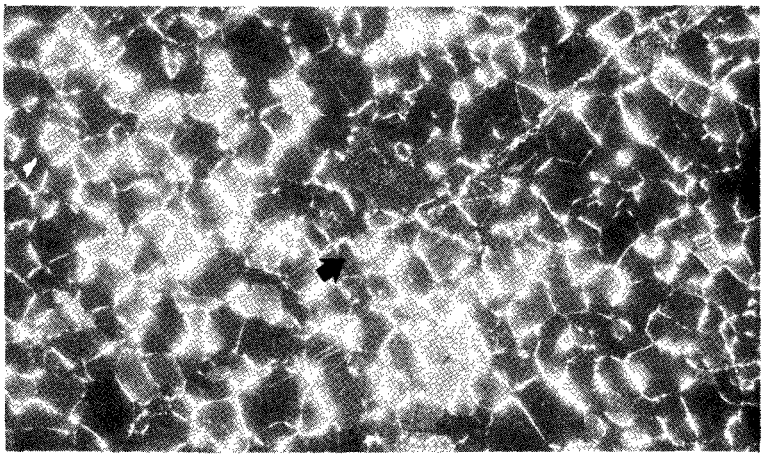

(b) Test temperature, -320° F (77° K); ratio of cycles applied to cycles to fracture, 0.25.

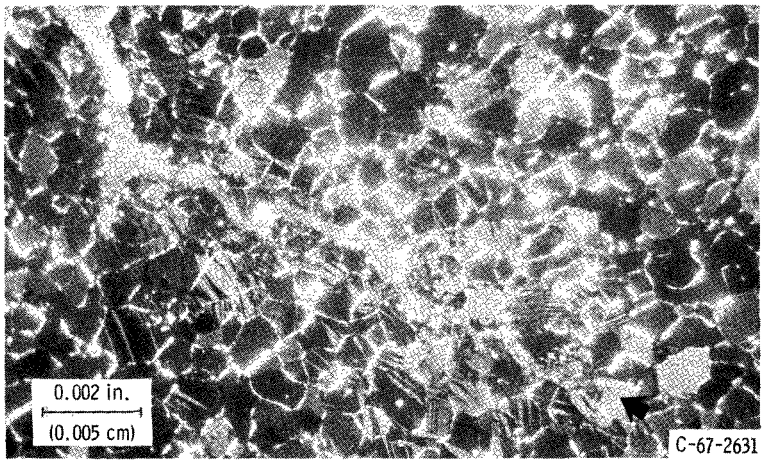

(c) Test temperature, 70° F (294° K); ratio of cycles applied to cycles to fracture, 0.6.

Figure 21. - Photomicrographs of areas surrounding crack tips in notched 5 Al-2.5 Sn-Ti alloy fatigue specimens. Twins in region adjacent to and in front of crack for samples tested at 70° F (294° K) and -452° F (4° K); specimens run (400 cycles) at maximum stress of 105 000 pounds per square inch (72 400 N/cm^2) and removed from test prior to fracture; etchant D.

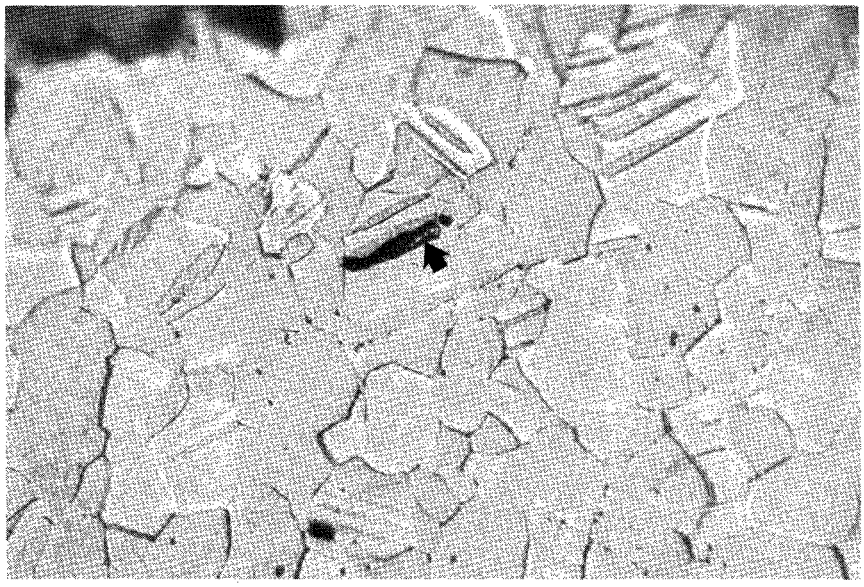

(a) Smooth specimen; life, 29 200 cycles.

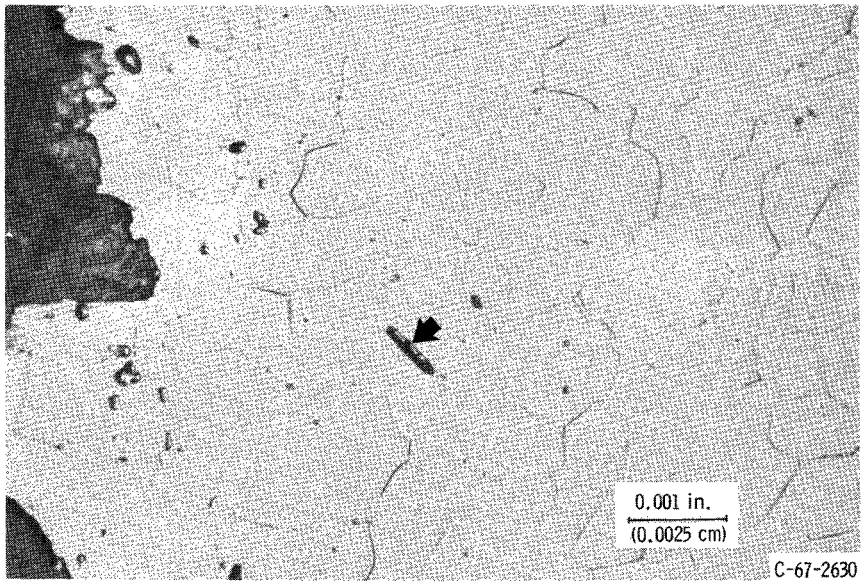

(b) Notched specimen; life, 14 cycles.

Figure 22. - Regions near fracture surface of 5 Al- 2.5 Sn-Ti fatigue specimens showing voids adjacent to twins after testing at -452° F (4° K). Etchant D.

section stress. Twinning in fatigue increased with increasing stress for this alloy; therefore, it might be expected that for the example shown in figure 21 fewer twins would occur at -320° F (77° K). The tendency for more twinning to occur in both notched tensile and fatigue-tested specimens than in smooth specimens may be due to the introduction of biaxial stresses that tend to suppress slip.

Although conclusive evidence of the possibly detrimental effect of twinning was not obtained, figure 22 illustrates voids in twinned regions of the microstructure near the fracture surface of specimens cycled at -452° F (4° K). The voids, indicated by arrows, although few in number, were located immediately adjacent to twins. It is possible that the voids could act as crack starters.

AISI 301 Stainless steel. - Macrographs of failed tensile specimens of AISI 301 stainless steel are shown in figure 23. Significantly greater elongation occurred at -320° F (77° K) than at the other test temperatures. The reduction in specimen area was virtually uniform along the entire test section after testing at -320° F (77° K). A small amount of localized necking occurred at the other test temperatures. Although not evident from the figure, Lüders lines were observed on the specimens after tensile tests at all temperatures. The plane of fracture at all temperatures was normal to the plane of the specimen.

The microstructure of the AISI 301 stainless steel sheet in the as-received (60 per-

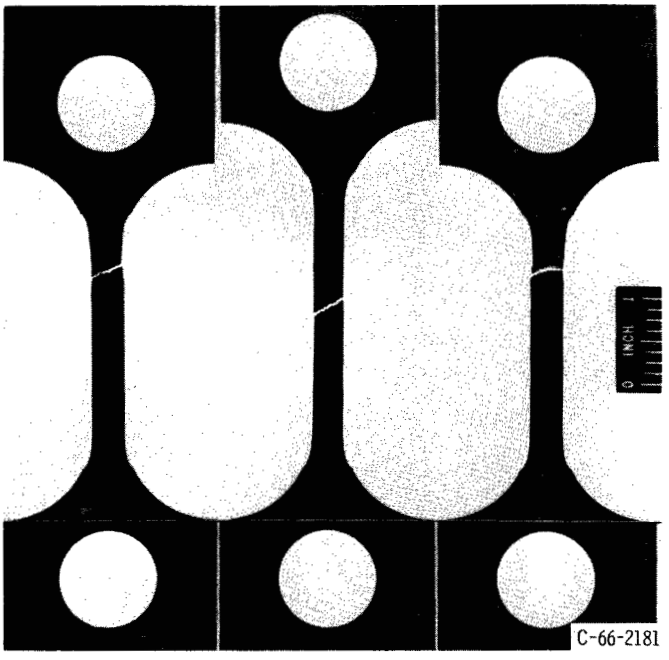

(a) 70° F (294° K). (b) -320° F (77° K). (c) -423° F (20° K).

Figure 23. - Macrophotographs of failed AISI 301 stainless steel tensile specimens showing characteristic fracture modes and final elongations for three test temperatures.

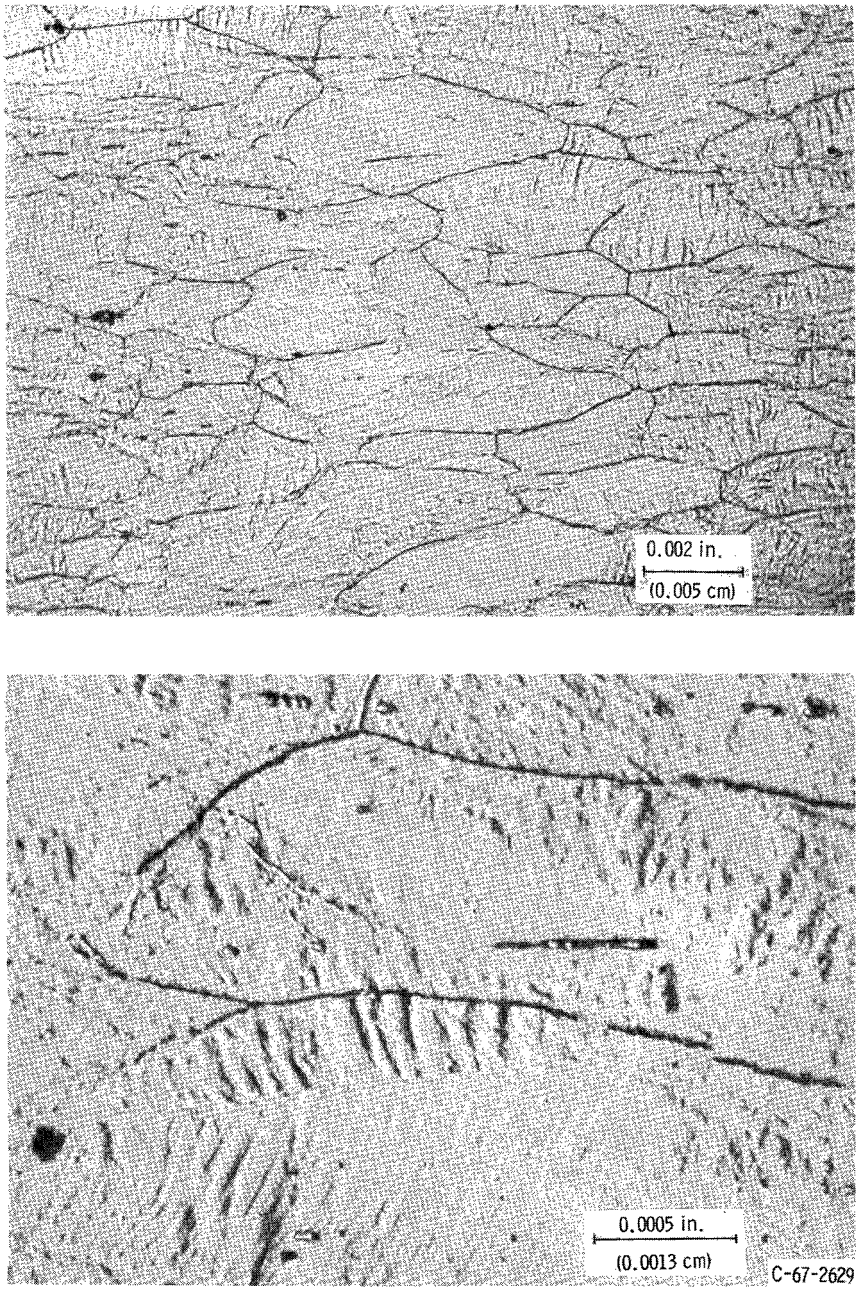

Figure 24. - Microstructure of as-received AISI 301 stainless steel sheet in 60 percent cold-rolled condition. Etchant E.

Test temperature,
°F (°K)

-423 (20)

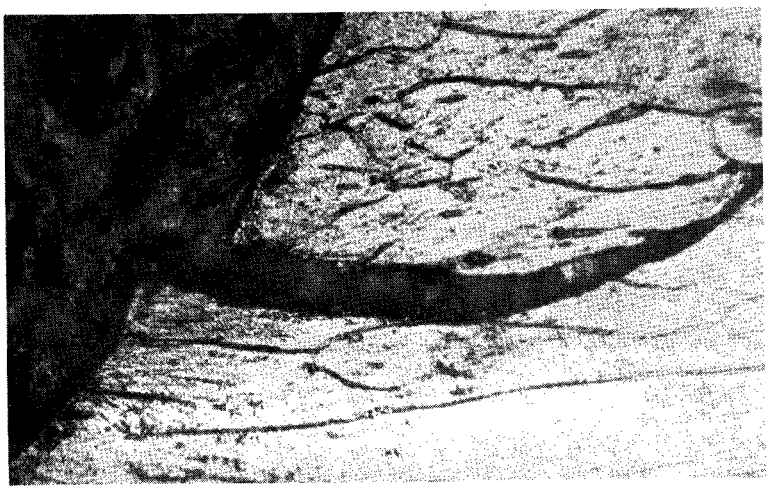

-320 (77)

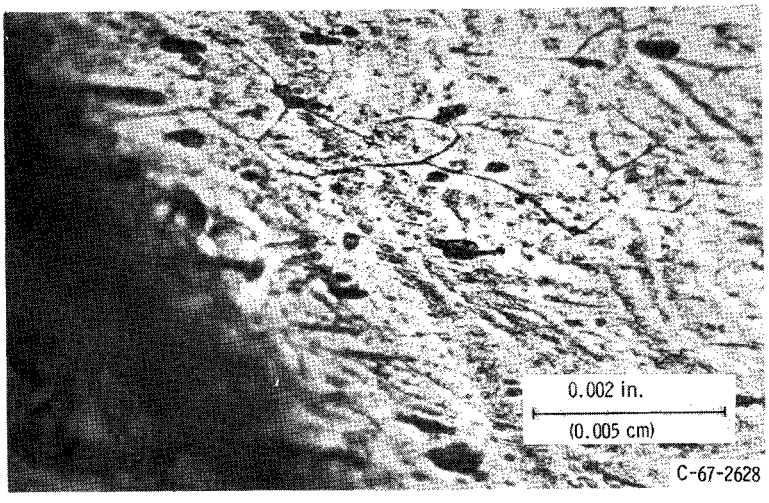

70 (294)

(a) Smooth specimens.

Figure 25. - Photomicrographs of zones immediately adjacent to fracture surface of AISI 301 stainless steel tensile specimens, illustrating mode of fracture. Etchant E.

Test temperature,
°F (°K)

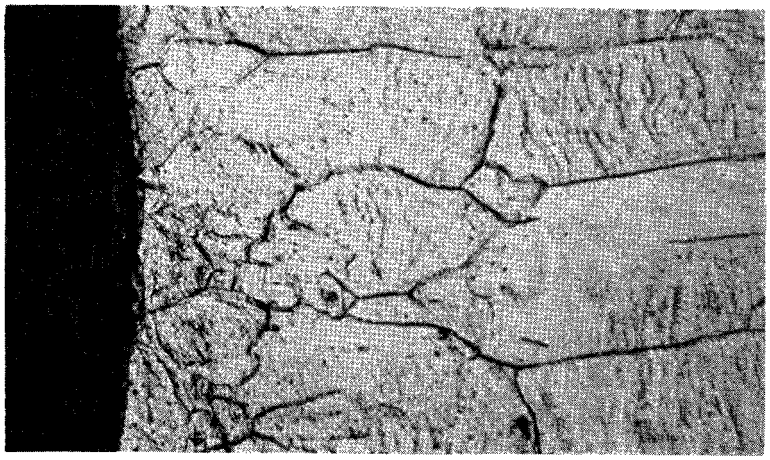

-423 (20)

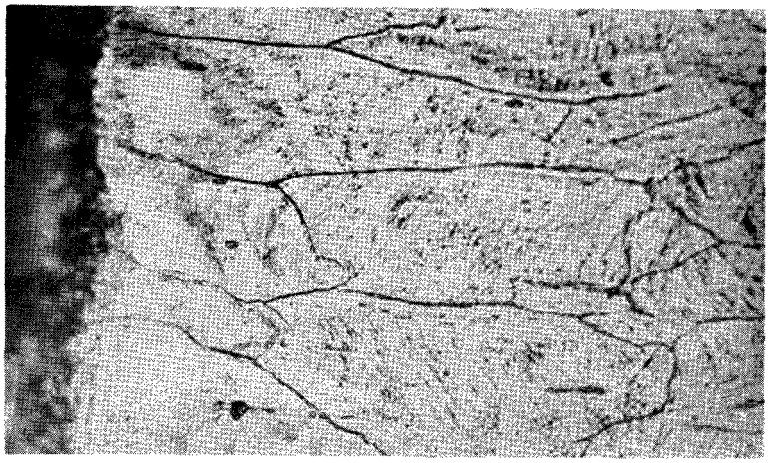

-320 (77)

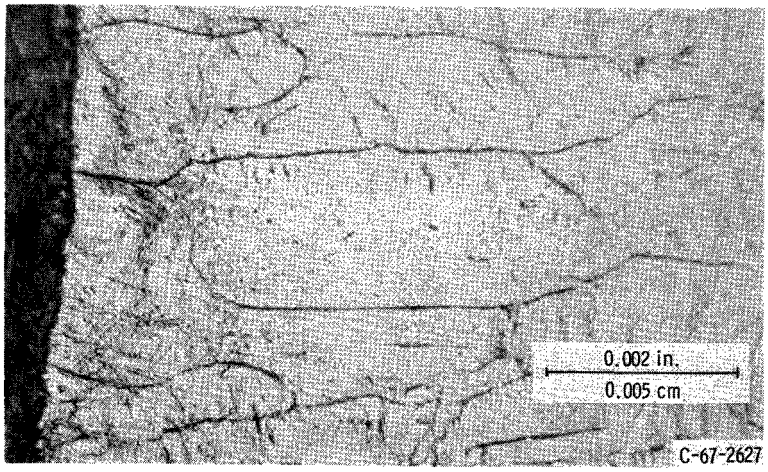

70 (294)

(b) Notched specimens.

Figure 25. - Concluded.

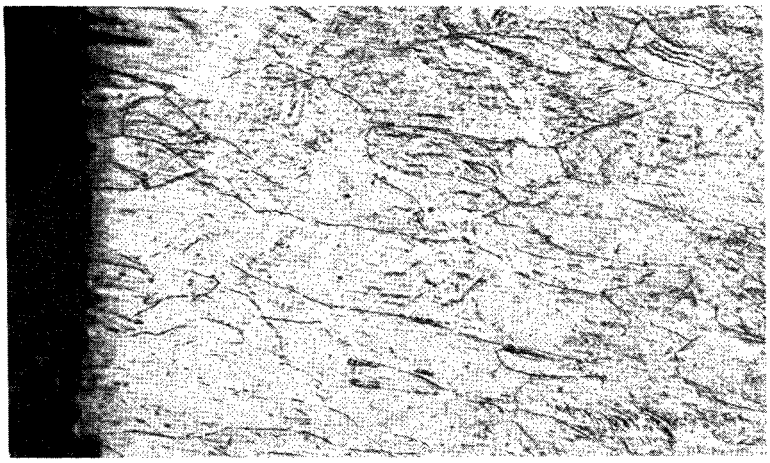

(a) Test temperature, -452° F (4° K).

(b) Test temperature, -320° F (77° K).

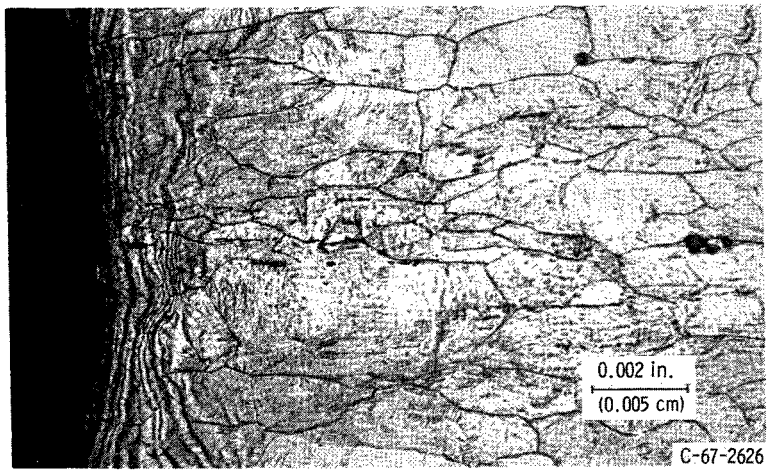

(c) Test temperature, 70° F (294° K).

Figure 26. - Photomicrographs of smooth fatigue specimens of AISI 301 stainless steel tested at maximum cyclic stress of 245 000 pounds per square inch (168 900 N/cm^2) showing fracture mode and disturbed regions adjacent to fracture. Etchant E.

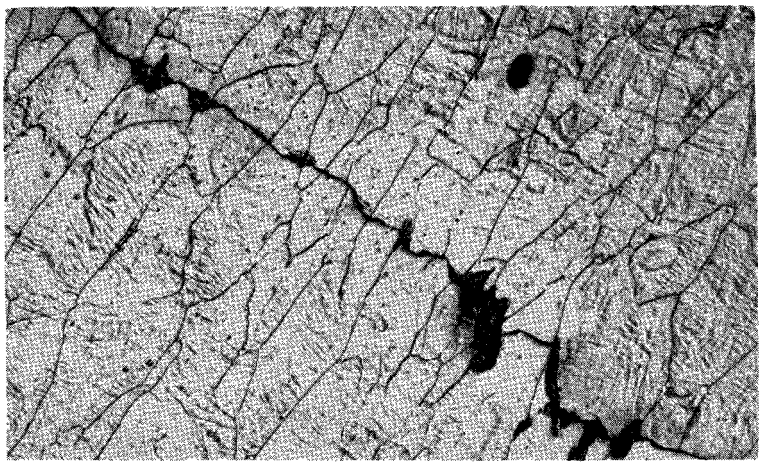

(a) Test temperature, -452° F (4° K); ratio of cycles applied to cycles to fracture, 0.7.

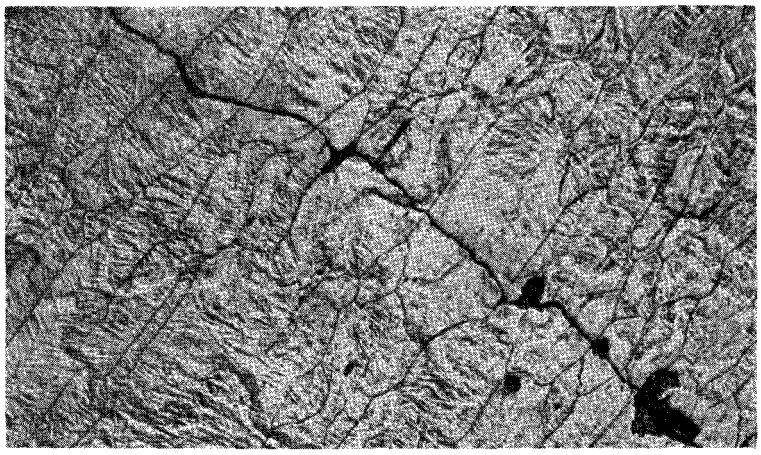

(b) Test temperature, -320° F (77° K); ratio of cycles applied to cycles to fracture, 0.14.

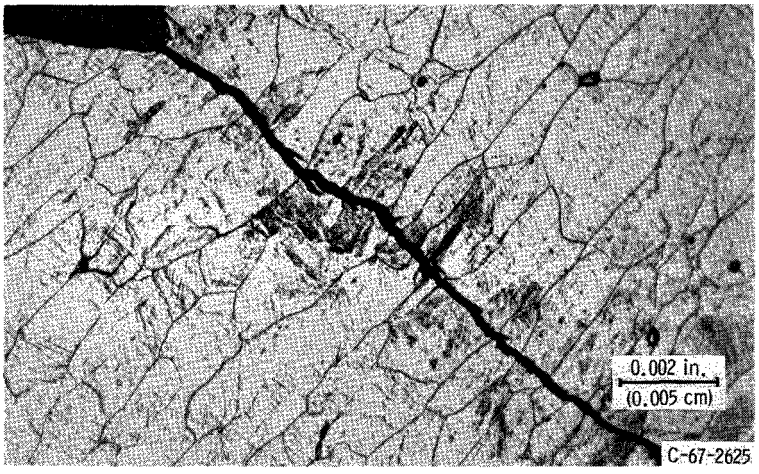

(c) Test temperature, 70° F (294° K); ratio of cycles applied to cycles to fracture, 0.15.

Figure 27. - Photomicrographs of notched fatigue specimens of AISI 301 stainless steel showing transgranular cracks. Maximum cyclic stress, 87 500 pounds per square inch (60 300 N/cm^2); tests stopped at 1100 cycles, before specimen failed; etchant E.

cent cold reduced) condition is shown in figure 24. The grains were elongated in the rolling direction. Attempts were made by means of X-ray diffraction to determine the relative amounts of austenite and martensite in untested specimens and in tested specimens. Qualitative results were obtained that showed that a greater amount of martensite than austenite was present in both tested and untested specimens. It was not possible to discern whether the test conditions altered the amount of austenite. It is interesting to note that other investigators (ref. 29) have shown that in 304 stainless steel the amount of transformed martensite increased with increasing tensile strain and that for a given strain a greater degree of transformation occurred as the temperature was decreased. The condition of that material (304 stainless steel) differed from the material in this investigation, however, in that it was in the annealed condition. The annealed material, being entirely austenitic, was more likely to exhibit significant transformation.

Figure 25 illustrates the microstructure of tensile specimens tested at each temperature. The regions immediately adjacent to the fracture surface are shown. The loading direction was horizontal with respect to the orientation of the micrographs. It is evident that cracking was transgranular in all cases. The microstructures of failed smooth fatigue specimens are shown in figure 26, and the microstructures of notched fatigue specimens that were removed from the test prior to complete separation are shown in figure 27. Some microstructural similarities between failed tensile and fatigue specimens are apparent. For example, all of the fractures were transgranular. There were disturbed regions immediately adjacent to the fracture surfaces in the smooth fatigue specimens (fig. 26) and in the smooth tensile specimens (fig. 25(a)). This type of disturbed region was not observed in the notched specimens. Finally, the plane of the fracture surfaces in the fatigue specimens (figs. 26 and 27) was normal to the loading axis, whereas it formed a steeper angle with respect to the loading axis in smooth tensile specimens.

SUMMARY OF RESULTS

An investigation was conducted to determine the cryogenic fatigue behavior of four candidate alloys for liquid rocket engines. Low-cycle fatigue data were obtained with smooth and notched (theoretical stress concentration factor $K_t > 17$) sheet specimens in ambient air, liquid nitrogen, and liquid helium in axial-tensile fatigue. Materials were 2014-T6 aluminum alloy, Inconel 718, 5 percent aluminum - 2.5 percent tin-titanium alloy (5Al-2.5Sn-Ti), and AISI 301 stainless steel. The minimum to maximum stress ratio (R factor) was 0.14. The following results were obtained:

1. Fatigue strength increased progressively with decreasing test temperature to -452° F (4° K) for all materials in the unnotched condition, except 301 stainless steel.

In the notched condition, the trend of increasing strength with decreasing temperature was observed in 2014-T6 aluminum alloy and Inconel 718.

2. The fatigue strength of smooth specimens was generally substantially higher than that of notched specimens for all materials at all temperatures over the entire cyclic life range.

3. Of the four materials considered, Inconel 718 and 301 stainless steel generally had the highest fatigue strength in both the unnotched and the notched condition. In the unnotched condition, their relative ranking varied depending on temperature and cyclic life, but in the notched condition, the fatigue strength of Inconel 718 was always greater or equal to that of AISI 301 stainless steel. The 5Al-2. 5Sn-Ti alloy and 2014-T6 aluminum alloy usually ranked third and fourth in fatigue strength regardless of specimen geometry.

4. When compared on the basis of fatigue-strength-to-density ratio, no single material was the best at all temperatures and cyclic lives. In most cases however, the strongest material was the 5Al-2. 5Sn-Ti alloy, although in the notched condition at lives greater than about 10^4 cycles the curves of fatigue-strength-to-density ratio for all materials tended to converge.

5. The fatigue notch factor K_f of all four materials increased with increasing cyclic life at all test temperatures. Up to 100 cycles, the fatigue notch factor was similar to the tensile notch factor for all materials and test temperatures considered, which suggests that the use of tensile notch factor might be adequate for design in low-cyclic-life applications. Inconel 718 generally had the lowest fatigue notch factors over the life range considered at all temperatures.

6. The concept of a functional relation between tensile and fatigue data was extended to both smooth and notched specimens for the materials of this investigation stress-cycled at cryogenic temperatures.

7. At all temperatures the mode of fracture in fatigue was generally transgranular for all materials.

8. Minor-phase-particle cracking was associated with fatigue failure in the 2014-T6 aluminum alloy at all temperatures. The crack that caused fracture passed through and linked certain minor phase particles. Although minor-phase-particle cracking was also observed in Inconel 718, the main crack that caused fracture did not preferentially pass through the cracked particles.

9. For the 5Al-2. 5Sn-Ti alloy, deformation by slip and by twinning was observed in both fatigue and tensile-tested specimens. Twinning was particularly marked at temperatures of -423° F (20° K) and -452° F (4° K) in both smooth and notched specimens.

Voids were observed adjacent to twins in specimens fatigue tested at -452° F (4° K), and may have contributed to fatigue cracking.

Lewis Research Center,
National Aeronautics and Space Administration,
Cleveland, Ohio, June 22, 1967,
129-03-08-01-22.

REFERENCES

1. Kropschot, R. H.; Parkerson, C. R.; O'Donel, J.; and Crum, M. G.: Low Temperature Tensile Testing Equipment and Results (300°-20° K). Rep. No. 2708, National Bureau of Standards, July 1, 1953.
2. Shank, M. E.; and Neimark, J. E.: Investigation of the Mechanism of Rapid Crack Propagation in Metals. Rep. No. DSR-7514, Dept. Mech. Eng., Massachusetts Inst. Tech., Aug. 15, 1958.
3. Rice, Leonard P.; Campbell, James E.; and Simmons, Ward F.: The Evaluation of the Effects of Very Low Temperatures on the Properties of Aircraft and Missile Metals. (WADD TR 60-254), Battelle Memorial Inst., June 1960.
4. Hanson, M. P.; Stickley, G. W.; and Richards, H. T.: Sharp-Notch Behavior of Some High-Strength Sheet Aluminum Alloys and Welded Joints at 75, -320, and -423° F. Symposium on Low-Temperature Properties of High-Strength Aircraft and Missile Materials. Spec. Tech. Pub. No. 287, ASTM, 1961, pp. 3-22.
5. Hanson, Morgan P.: Smooth and Sharp-Notch Tensile Properties of Cold-Reduced AISI 301 and 304L Stainless-Steel Sheet at 75°, -320°, and -423° F. NASA TN D-592, 1961.
6. DeMoney, F. W.: Performance of a New Cryogenic Aluminum Alloy, 7039. Advances in Cryogenic Engineering. Vol. 9, K. D. Timmerhaus, ed., Plenum Press, 1964, pp. 112-123.
7. Watson, J. F.; and Christian, J. L.: Low-Temperature Properties of K-Monel, Inconel-X, René 41, Haynes 25, and Hastelloy B Sheet Alloys. J. Basic Eng., vol. 84, no. 2, June 1962, pp. 265-277.
8. Achbach, W. P.; and Favor, R. J.: Design Properties as Affected by Cryogenic Temperatures (Ti-6Al-4V, AISI 4340, and 7079-T6 Alloys). DMIC Memo 81, Battelle Memorial Inst., Jan. 24, 1961.

9. Martin, H. L.; Imgran, A. G.; and Lyman, W. S.: Effects of Low Temperatures on Structural Metals. Battelle Memorial Inst. NASA SP-5012, 1964.

10. Anderson, W. A.; Kaufman, J. G.; and Kane, J. E.: Notch Sensitivity of Aluminum-Zinc-Magnesium Alloys at Cryogenic Temperatures. Advances in Cryogenic Engineering. Vol. 9, K. D. Timmerhaus, ed., Plenum Press, 1964, pp. 104-111.

11. Shannon, J. L., Jr.; and Brown, W. F., Jr.: Effects of Several Production and Fabrication Variables on Sharp Notch Properties of 5Al-2.5Sn-Titanium Alloy Sheet at Liquid Hydrogen Temperature. ASTM Proc., vol. 63, 1963.

12. Desisto, T. S.; and Carr, F. L.: Low Temperature Mechanical Properties of 300 Series Stainless Steel and Titanium. Monograph Series MS-22, Watertown Arsenal Labs., Aug. 1960.

13. Schwartzberg, F. R.; Osgood, S. H.; Keys, R. D.; and Kiefer, T. F.: Cryogenic Materials Data Handbook. (AFML-TDR-64-280, DDC No. AD-609562), Martin Co., Aug. 1964.

14. Spretnak, J. W.; Fontana, M. G.; and Brooks, H. E.: Notched and Unnotched Tensile and Fatigue Properties of Ten Engineering Alloys at 25° C and -196° C. Trans. ASM, vol. 43, 1951, pp. 547-570.

15. Fontana, M. G.; Bishop, S. M.; and Spretnak, J. W.: Investigation of Mechanical Properties and Physical Metallurgy of Aircraft Alloys at Very Low Temperatures. Part 5. Mechanical Properties of Metals and a Plastic Laminate at Low Temperatures. (WADC TR 5662 pt. 5), Ohio State Univ., Research Foundation, Dec. 1953.

16. McCammon, R. D.; and Rosenberg, H. M.: The Fatigue and Ultimate Tensile Strengths of Metals Between 4.2 and 293° K. Proc. Roy. Soc. (London), Ser. A, vol. 242, no. 1229, Oct. 29, 1957, pp. 203-211.

17. MacCrone, R. K.; McCammon, R. D.; and Rosenberg, H. M.: The Fatigue of Metals at 1.7° K. Phil. Mag., vol. 4, no. 38, Feb. 1959, pp. 267-268.

18. Favor, R. J.; Gideon, D. N.; Grover, H. J.; Hayes, J. E.; and McClure, G. M.: Investigation of Fatigue Behavior of Certain Alloys in the Temperature Range Room Temperature to -423° F. (WADD TR 61-132), Battelle Memorial Inst., June 1961.

19. Gideon, Donald N.; Favor, Ronald J.; Koppenhafer, Arthur; Grover, Horace J.; and McClure, George M.: Investigation of Notch Fatigue Behavior of Certain Alloys in the Temperature Range of Room Temperature to -423° F. (AF ASD-TDR-62-351), Battelle Memorial Inst., Aug. 1962.

20. Christian, J. L.: Physical and Mechanical Properties of Pressure Vessel Materials for Application in a Cryogenic Environment. (AF ASD-TDR-62-258), General Dynamics/Astronautics, Mar. 1962.

21. Hilsen, R. R.; Yen, C. S.; and Whiteson, B. V.: Low Cycle Fatigue of Ti-6Al-4V at -423° F. Symposium on Fatigue Tests of Aircraft Structures: Low-Cycle, Full-Scale, and Helicopters. Spec. Tech. Pub. No. 338, ASTM, 1963, pp. 62-75.

22. Schwartzberg, F. R.; Kiefer, T. F.; and Keys, R. D.: Determination of Low-Temperature Fatigue Properties of Structural Metal Alloys. Rep. No. CR-64-74 (NASA CR-59839), Martin Co., Oct. 1964.

23. Kiefer, T. F.; Keys, R. D.; and Schwartzberg, F. R.: Determination of Low-Temperature Fatigue Properties of Structural Metal Alloys. Rep. No. CR-65-70 (NASA CR-67818), Martin Co., Oct. 1965.

24. Peterson, Rudolph E.: Stress Concentration Design Factors. John Wiley & Sons Inc., 1953.

25. Klima, Stanley J.; Nachtigall, Alfred J.; and Hoffman, Charles A.: Preliminary Investigation of Effect of Hydrogen on Stress-Rupture and Fatigue Properties of an Iron-, a Nickel-, and a Cobalt-Base Alloy. NASA TN D-1458, 1962.

26. Manson, S. S.: Fatigue: A Complex Subject - Some Simple Approximations. Experimental Mech., vol. 5, no. 7, July 1965, pp. 193-226.

27. Anon.: Tentative Methods of Preparation of Metallographic Specimens. ASTM Standard E 3-58T, 1958.

28. Pelloux, Regis M. N.: Influence of Constituent Particles on Fatigue Crack Propagation in Aluminum Alloys. Rep. No. D 1-82-0297, Boeing Scientific Research Lab., Sept. 1963. (Available from DDC as AD-423026).

29. Guntner, C. J.; and Reed, R. P.: The Effect of Experimental Variables Including the Martensitic Transformation on the Low Temperature Mechanical Properties of Austenitic Stainless Steels. Trans. ASM, vol. 55, no. 3, Sept. 1962, pp. 399-419.

"The aeronautical and space activities of the United States shall be conducted so as to contribute . . . to the expansion of human knowledge of phenomena in the atmosphere and space. The Administration shall provide for the widest practicable and appropriate dissemination of information concerning its activities and the results thereof."

—NATIONAL AERONAUTICS AND SPACE ACT OF 1958

NASA SCIENTIFIC AND TECHNICAL PUBLICATIONS

TECHNICAL REPORTS: Scientific and technical information considered important, complete, and a lasting contribution to existing knowledge.

TECHNICAL NOTES: Information less broad in scope but nevertheless of importance as a contribution to existing knowledge.

TECHNICAL MEMORANDUMS: Information receiving limited distribution because of preliminary data, security classification, or other reasons.

CONTRACTOR REPORTS: Scientific and technical information generated under a NASA contract or grant and considered an important contribution to existing knowledge.

TECHNICAL TRANSLATIONS: Information published in a foreign language considered to merit NASA distribution in English.

SPECIAL PUBLICATIONS: Information derived from or of value to NASA activities. Publications include conference proceedings, monographs, data compilations, handbooks, sourcebooks, and special bibliographies.

TECHNOLOGY UTILIZATION PUBLICATIONS: Information on technology used by NASA that may be of particular interest in commercial and other non-aerospace applications. Publications include Tech Briefs, Technology Utilization Reports and Notes, and Technology Surveys.

Details on the availability of these publications may be obtained from:

SCIENTIFIC AND TECHNICAL INFORMATION DIVISION

NATIONAL AERONAUTICS AND SPACE ADMINISTRATION

Washington, D.C. 20546